communications biology

Article

https://doi.org/10.1038/s42003-024-06860-9

Mycobacterium marinum MMAR_0267-regulated copper utilization facilitates bacterial escape from phagolysosome

Check for updates

Junqi Xu[1], Shaying Ma[2], Yu Huang[3], Qiao Zhang[3], Lingxi Huang[3], Hongxiang Xu[3], Ismail Mohamed Suleiman[3], Peibo Li[2] ✉, Zhijian Wang[1] ✉ & Jianping Xie[1,2] ✉

The host limits *Mycobacterium tuberculosis* (*Mtb*) by enriching copper in high concentrations. This research investigates how *Mtb* escapes copper stress. The membrane protein encoded by *Mtb Rv0102*, when its homolog in *M. smegmatis* (*MSMEG_4702*) was knocked out, resulted in a fourfold decrease in intracellular copper levels and enhanced tolerance to elevated extracellular copper concentrations. Similarly, knockout mutants of its homolog in *M. marinum* (*MMAR_0267*) showed increased virulence in zebrafish and higher bacterial load within macrophages. In THP-1 cells infected with *MMAR_0267* deletion mutants, the intracellular survival of these mutants increased, along with reduced THP-1 cell apoptosis. Deficiency in copper down-regulated the transcriptional level of the virulence factor CFP-10 in *M. marinum*, suppressed cytosolic signaling via the macrophage STING pathway, leading to decreased production of IFN-β and reduced cell apoptosis. In conclusion, these findings highlight the significant impact of copper on the survival and reproduction of mycobacteria, underscoring the importance of studying mycobacterial adaptation mechanisms in copper-rich environments.

In the natural environment, trace metal elements such as manganese (Mn), copper (Cu), iron (Fe), zinc (Zn), and nickel (Ni) serve as inhibitors of *Mycobacterium tuberculosis* (*Mtb*) growth by exerting damage to cell membranes, interfering with metabolic processes, and inducing oxidative stress[1]. These metals play key roles in protein folding and enzyme activity, but their excess accumulation can be toxic[2]. The host has evolved mechanisms to sequester vital metals like Mn, Fe, and Zn within phagosomes to impede the growth of intracellular pathogens. Conversely, the surplus copper is harnessed by host cells to counteract intracellular pathogens[3]. Therefore, maintaining metal, including copper, homeostasis is critical for intracellular pathogen survival.

Tuberculosis, resulting from *Mtb* infection, remains a substantial global public health challenge[4]. Copper, alongside other metal elements, is crucial for *Mtb* replication and enzyme function[5]. copper ions act as catalysts in single-electron transfer reactions within the cytochrome respiratory enzyme aa3-bc1 complex[6]. The redox potential of Cu(II)/ Cu(I) surpasses that of Fe(III)/Fe(II)[7], leading to reactive oxygen species (ROS) generation upon copper entry into bacterial cells like Mycobacterium avium, leading to DNA damage and cellular integrity compromise[8]. Copper toxicity arises from its competitive binding with metalloproteins, potentially inactivating critical enzymes and hindering *Mtb* growth[9]. To counteract the toxicity from excess copper, *Mtb* employs cytoplasmic proteins including metallothioneins, copper storage proteins[10], and copper efflux proteins to chelate or buffer copper ions[11]. *Mtb* possesses a sophisticated copper ion uptake system to regulate intracellular copper balance.

Cross-membrane copper transport relies on specific membrane proteins that facilitate copper ion transfer. In *Mtb*, one such protein is CopA, a member of the P1B-1 type ATPase subfamily. CopA is vital for transferring copper from ATPase to cytochrome oxidase, determining copper importation or expulsion from the cell[12]. In the presence of excess copper, the CopZ/A operon induces a copper efflux system. CopZ, acting as a copper chaperone, transfers copper to the CPX-type efflux ATPase CopA[13]. Additionally, the CtpA gene is induced during *Mtb* infection. *Mtb* CtpA, CtpB, and CtpV are transmembrane proteins involved in heavy metal cation transport, with CtpA potentially serving as a copper transporter across the mycobacterial membrane[14]. CsoR, a copper-inducible transcriptional regulator, controls copper efflux factors like CtpV in *Mtb*, regulating intracellular copper ion levels[15,16]. This copper homeostasis system is conserved in various bacteria

[1]Key Laboratory of Freshwater Fish Reproduction and Development, Ministry of Education, Key Laboratory of Aquatic Science of Chongqing, Institute of Modern Biopharmaceuticals, School of Life Sciences, Southwest University, Chongqing, 400715, China. [2]Chongqing Public Health Medical Center, Chongqing, China. [3]Chongqing Emergency Medical Center, Chongqing the Fourth Hospital, Jiankang Road, Yuzhong, Chongqing, 400014, China. ✉e-mail: 157318851@qq.com; wangzj1969@126.com; georgex@swu.edu.cn

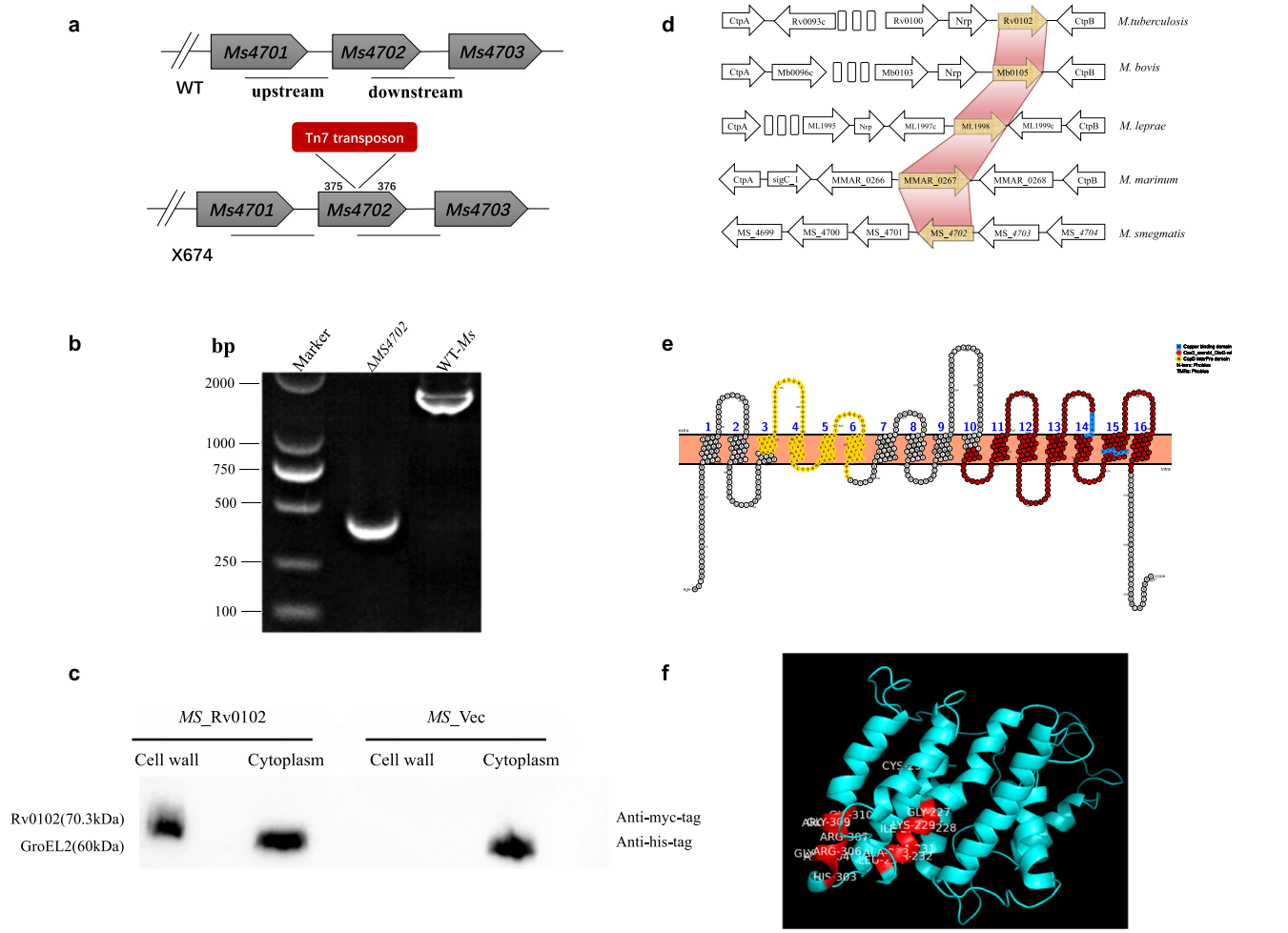

Fig. 1 | Genomic locus of the ΦMycoMar insertion. a Shows the chromosomal position of *MSMEG_4702* in *M. smegmatis* mc^{2}155, with Tn7 transposons inserted between the 375th and 376th positions of the *MS4702* gene via phage transduction. **b** Confirms the presence of the *MSMEG_4702* gene in WT_Ms and Δ*MSMEG_4702* cultures grown to OD_{600} = 0.8 through PCR amplification. **c** Presents the Western blot identification of *Rv0102* associated with the *M. smegmatis* cell wall, determined by cell fractionation experiments. GroEL2 was used as a cytoplasmic marker. **d** Depicts the genomic context of Rv0102 in mycobacteria, highlighting conserved regions across mycobacterial genomes. Arrows indicate gene transcription. **e** Displays the sequence analysis of the Cu transporter Rv0102, detailing conserved functional domains and structural domains including 16 transmembrane domains. **f** Shows a model predicting copper binding sites based on the amino acid sequence of the Rv0102 protein.

beyond *Mtb*, including *Streptococcus*, *Salmonella*, and *Escherichia coli*[10,17]. The mechanism of copper(I) transport across bacterial membranes remains unclear[18]. Recent studies highlight the essential role of the p-type ATPase CtpB in copper acquisition and respiration, with its absence linked to increased virulence[6]. Nonetheless, a stable and regulated copper uptake pathway is crucial for Mycobacteria to maintain copper ion homeostasis.

This study shows that the ABC transporter Rv0102, located on the cell membrane, along with its homologous genes *MMAR_0267* in *M. marinum* and *MSMEG_4702* in *M. smegmatis*, play a crucial role in regulating intracellular copper levels and are integral components of the copper homeostasis system in *Mtb*. When the homologous gene *MSMEG_4702* in *M. smegmatis* is deleted, it results in a significant impairment of the bacterium's ability to effectively utilize copper ions. The deletion mutants exhibit increased tolerance to higher concentrations of copper ions. Likewise, the elimination of the homologous gene *MMAR_0267* in *M. marinum* also significantly affects the bacterium's capacity to utilize copper. The underutilization of copper resources increases the survival and virulence of the deletion strain in zebrafish and decreases the THP-1 macrophages apoptosis, possibly due to macrophages failure to use copper ions to kill the engulfed *Mm*. Our study presents the initial evidence indicating that *Mtb* Rv0102 is a membrane protein involved in the utilization of copper ions.

Results

Rv0102 is involved in copper ions transfer

To generate an adequate number of single mutants, we created a mutant library of *M. smegmatis* mc^2 155 with 20,000 transposon insertions using the Tn7 transposon system. The library was screened on 7H10 medium with high copper ion concentration (20 μmol/L $CuSO_4$), leading to the identification of a copper-tolerant mutant X674. This mutant had a Tn7 transposon insertion between the 375th and 376th positions of *M. smegmatis MSMEG_4702*, confirmed by hiTAIL-PCR and BLAST. To validate the phenotype, we deleted the *MSMEG_4702* gene in *M. smegmatis* mc^2 155 via homologous chromosome exchange (Fig. 1b) and complemented it with the *Mtb* homolog gene *Rv0102*, which corresponds to *MSMEG_4702* in *Mtb* (Supplementary Fig. 1). Multiple-sequence alignment analysis showed high conservation of the *MSMEG_4702* amino acid sequence across various mycobacterial species (Fig. 1d). There is also significant homology between the DNA and amino acid sequences (Supplementary Fig. 2).

The *Rv0102* gene in *Mtb* is annotated as an integral membrane protein containing 661 amino acids (1986bp), while *MSMEG_4702* in *M. smegmatis* is annotated as an ABC-type transporter, indicating that Rv0102 might function as a transporter in the cytoplasmic membrane. Protein immunoblotting brought about the localization of the Rv0102

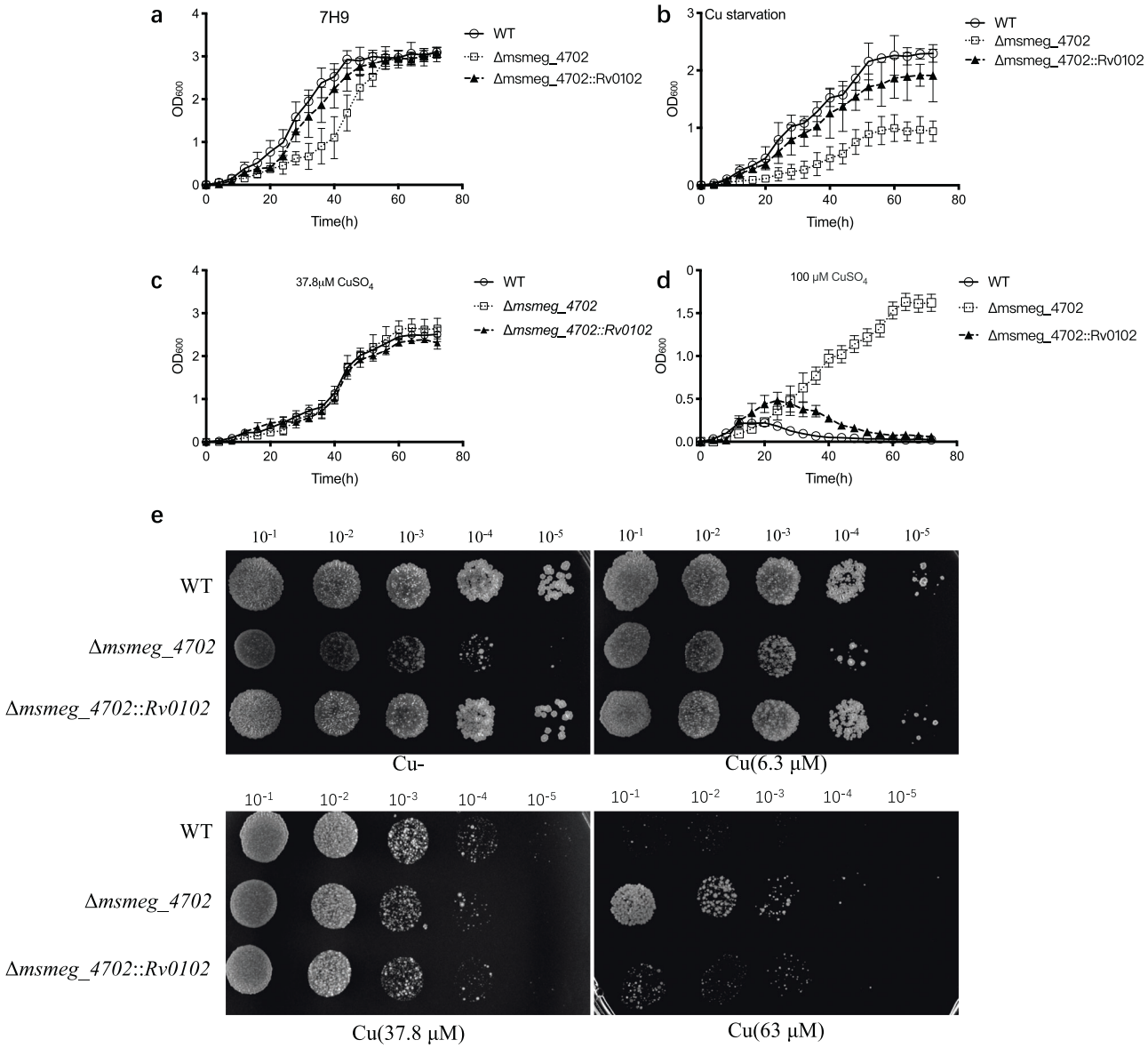

Fig. 2 | Growth difference of WT and Δ*MSMEG_4702* strains under different copper conditions. WT-Ms, Δ*MSMEG_4702* deletion mutant, and complemented strains were cultured in different media conditions: (**a**) Pure 7H9 medium, (**b**) Copper-free 7H9 medium without $CuSO_4$, (**c**) Copper-free 7H9 medium with 37.8 μmol/L $CuSO_4$, and (**d**) Copper-free 7H9 medium with 100 μmol/L $CuSO_4$. Error bars represent standard deviation($n = 3$). **e** Copper sensitivity was assessed by spotting serial dilutions of log-phase cultures of WT-*Ms*, Δ*MSMEG_4702* mutant X674, and complemented strains on solid copper-free 7H9 medium with varying $CuSO_4$ concentrations —6.3 μmol/L, 37.8 μmol/L, and 63 μmol/L.

protein, showing its exclusive presence in the cell wall/cell membrane (CW/CM) fraction while being absent in the cytoplasmic (CP) fraction (Fig. 1c), indicating that Rv0102 is a protein associated with the cell envelope. According to the analysis results of the PPM server[19], Rv0102 has 16 transmembrane segments (TMS), with potential copper-binding motifs in TMS14 to TMS15. InterProScan results suggested a conserved homeodomain in TMS3 to TMS6, akin to CopD, and cytochrome oxidase characteristics in TMS11 to TMS16 (Fig. 1e). CopD, a cytoplasmic copper transfer protein with no Mycobacterium homologs, hints at *Mtb* Rv0102 possibly having a copper uptake role like CopD. Protein structure predictions via I-TASSER and PyMOL indicated potential copper ion binding sites with features of divalent cation transport (Fig. 1f). The absence of *MSMEG_4702* in *M. smegmatis* confers high copper tolerance, suggesting *MSMEG_4702*'s crucial involvement in facilitating divalent copper ion transport in *Mtb*.

The deficiency of MSMEG_4702 confers copper tolerance to *M. smegmatis*

Copper ions are essential for *Mycobacterium* virulence[20]. In contrast to the wild-type (WT) strain, the deletion mutant Δ*MSMEG_4702* strain exhibited growth defects in Middlebrook 7H9 liquid medium supplemented with 0.05% Tween80 and 0.2% glycerol (Fig. 2a). The knockout *MSMEG_4702* strain resulted in a delayed growth of the Δ*MSMEG_4702* strain compared to the WT strain after 8 h of culture. However, after an extended culture (64 h), the bacterial densities of both the Δ*MSMEG_4702* and WT strains tended to reach a similar level. To eliminate the potential effects of copper present in the commercial Middlebrook 7H9 medium, a copper-free 7H9 medium (Use Middlebrook7H9 recipe, exclude $CuSO_4$) was prepared for a growth comparison. As anticipated, the growth defect of the Δ*MSMEG_4702* strain became significantly more severe after 64 h of cultivation in the copper-free 7H9 medium, exhibiting a much greater delay

compared to the WT strain (Fig. 2b). The observed phenotype provides strong evidence for the involvement of *MSMEG_4702* in copper ion utilization. Surprisingly, both the wild-type and complemented strains were capable of growth in copper-free Middlebrook 7H9 media, suggests that copper's fate within bacteria involves its binding to copper-storing proteins such as MymT. These proteins play a crucial role in mitigating copper toxicity under excessive copper conditions and can also serve as a source of copper nutrition during copper scarcity. Additionally, *MSMEG_4702* is not the only protein involved in copper uptake. Subsequent to the knockout of CtpB, a validated copper-uptake-associated protein[6], growth defects were noted in two strains under copper-deficient conditions (Supplementary Fig. 3F). Nonetheless, the deficiencies induced by the knockout of the *MMAR_0267* homologous gene, corresponding to *MSMEG_4702*, seem to be more pronounced, indicating a more critical role for MSMEG_4702 in facilitating copper uptake in mycobacterium.

When copper ion is excessive, copper could be transferred into the cytoplasm through specific copper transport systems in the membrane, such as the major facilitator superfamily (MSF) transporters[21]. $CuSO_4$ of different concentrations (37.8 μM and 100 μM respectively) were added into the copper-free 7H9 medium and bacterial growth was evaluated again. Interestingly, the growth curves of WT and Δ*MSMEG_4702* strains were essentially identical in the presence of 37.8 μmol/L $CuSO_4$ (Fig. 2c). However, when the concentration of $CuSO_4$ reached 100 μmol/L, both WT and complemented strains entered the decline phase, while the Δ*MSMEG_4702* strain remained in the logarithmic phase (Fig. 2d). The slower growth of the mutant in a low copper environment may be due to its significantly reduced ability to absorb and utilize copper, which adversely affects its growth. Instead, the mutant's resistance to a high copper environment is the result of its impaired copper absorption, preventing excessive accumulation and thus reducing susceptibility to high copper toxicity. This indicates that *M. smegmatis* MSMEG_4702 is indeed involved in the utilization of copper ions, and the reduction in copper utilization resulting from the deletion of *MSMEG_4702* enables the mutant strain to survive in high concentrations of exogenous copper.

We investigated the impact of copper on bacterial growth on solid medium lacking copper ions and observed a significant growth rate impairment in the Δ*MSMEG_4702* strain (Fig. 2e). $CuSO_4$ at concentrations of 6.3 μmol/L, 37.8 μmol/L, and 63 μmol/L were added to copper-free 7H9 solid medium, inoculated with 10 μl of diluted bacterial solution. Results showed that increasing $CuSO_4$ concentration notably inhibited WT strain growth. Conversely, Δ*MSMEG_4702* growth was enhanced with rising $CuSO_4$ levels (Fig. 2e). At 37.8 μmol/L $CuSO_4$, both WT and Δ*MSMEG_4702* strains exhibited similar growth levels. Moreover, at 63 μmol/L $CuSO_4$, Δ*MSMEG_4702* strain displayed normal growth while WT could not survive. These findings suggest that the protein encoded by *M. smegmatis MSMEG_4702* is crucial for copper ion utilization.

MSMEG_4702 deficiency impairs the growth of *M. smegmatis* by reducing intracellular copper concentrations and inhibiting cell division

Using the superpresence microplate method, we assessed the intracellular copper ion levels of both WT and Δ*MSMEG_4702* strains. WT *M. smegmatis* maintained stable intracellular copper ion concentrations around 0.08 μmol/L, unaffected by external $CuSO_4$ concentration changes (Fig. 3a). However, at 37.8 μmol/L $CuSO_4$, WT intracellular copper levels rose, suggesting *M. smegmatis* can regulate copper homeostasis to support growth. In cases of excessive extracellular copper reaching bactericidal levels, *M. smegmatis* may encounter homeostasis failure, leading to a sharp intracellular copper increase hindering bacterial growth. Notably, Δ*MSMEG_4702* strain showed significantly lower intracellular copper content compared to WT, independent of external $CuSO_4$ levels (Fig. 3a). Conversely, very high $CuSO_4$ concentrations (63 μmol/L) resulted in six times higher intracellular copper levels in WT vs. Δ*MSMEG_4702*. Rv0102 complementation successfully restored Δ*MSMEG_4702* intracellular copper levels, emphasizing Rv0102's vital role in copper ion regulation. Zinc ion addition did not yield significant differences (Supplementary Fig. 4A). Overall, our data suggest Δ*MSMEG_4702* markedly impairs copper ion utilization in *M. smegmatis*.

Interestingly, despite the significant intracellular copper content difference, no distinct growth variation was observed between WT and Δ*MSMEG_4702* strains on solid medium (Fig. 2e) or liquid medium (Fig. 2c) at 37.8 μM $CuSO_4$ concentration. WT intracellular copper ion concentration was four times higher than Δ*MSMEG_4702*, restorable by *Rv0102* complementation (Fig. 3a). Our data indicated a critical transition threshold of copper from growth promoter to inhibitor in *M. smegmatis* lying between 0.1 μmol/L and 0.2 μmol/L. At this pivotal copper concentration, Δ*MSMEG_4702* growth was boosted while WT strain growth was notably hindered. Despite the growth behavior contrast, both strains ultimately reached similar growth levels. In summary, these findings highlight *MSMEG_4702*'s crucial role in mediating environmental copper ion utilization, maintaining copper homeostasis, and fostering *M. smegmatis* growth.

Based on our experimental studies, we explored the impact of copper on bacterial proliferation and its influence on the growth or division of Δ*MSMEG_4702*. Under optimal $CuSO_4$ levels, the wild-type *M. smegmatis* displayed distinctive colony morphology with large, rounded single colonies (Supplementary Fig. 4B). Supplementing copper-free 7H9 culture medium with different copper concentrations (0 μmol/L, 6.3 μmol/L, 37.8 μmol/L, and 126 μmol/L) revealed reduced growth rates and smaller colony sizes for Δ*MSMEG_4702* at 0 μmol/L or 6.3 μmol/L $CuSO_4$, while the growth rate and colony size of the wild type remained normal. Under 37.8 μmol/L $CuSO_4$, both the wild type and Δ*MSMEG_4702* exhibited comparable growth rates and colony sizes. Interestingly, exposure to 126 μmol/L $CuSO_4$ led to WT growth failure but allowed Δ*MSMEG_4702* growth (Fig. 3b). Copper deficiency impairs bacterial growth enzymes by disrupting their function, possibly because copper ions serve as essential cofactors[22]. When cultured with 6.3 μmol/L $CuSO_4$, Δ*MSMEG_4702* displayed slightly elongated and more dispersed morphology (Fig. 3c), whereas the wild-type strain exhibited uniform length. To reference data for CtpB at the same time, we tested the accumulation of DNA damage in Δ*MMAR_0267* and Δ*Ctp*B with *Mycobacterium marinum*. TUNEL experiment results showed that the accumulation of DNA damage in Δ*MMAR_0267* at low copper concentrations was higher than that of the wild type, and there was no significant difference in Δ*Ctp*B, while at higher copper concentrations, Δ*MMAR_0267* exhibited lower DNA damage (Fig. 3d). Based on the findings, it can be concluded that MMAR_0267 has a greater impact on the intracellular copper ion content in bacteria compared to CtpB. Copper/zinc superoxide dismutase (SodC), in which copper ions participate, plays an important role in protecting cells from oxidative damage during bacterial cell division and is conducive to normal growth and division[23]. Therefore, we examined the expression of SodC and the cuprous enzyme cytochrome c oxidase, which is required for growth in vitro. Lack of MMAR_0267 reduced SodC expression at normal copper concentrations (6.3 μM $CuSO_4$), but no difference at high copper concentrations (63 μM $CuSO_4$) (Fig. 3e). Therefore, the reason for the increase in DNA damage caused by MMAR_0267 deficiency under normal copper concentration levels may be that insufficient copper uptake reduces the expression of SodC. However, at high copper concentrations, SodC does not overexpress, leading to lower DNA damage. It is hypothesized that other copper-regulated enzymes are responsible for clearing oxidative damage. Iron-sulfur clusters, common in proteins, encompass a variety of structures, including basic [2Fe–2S] and [4Fe–4S] forms, as well as complex configurations in enzymes such as nitrogenase and hydrogenase, which are involved in cell division and maintaining the redox balance within mycobacteria, helping the bacteria to resist oxidative stress from the external environment[24–26]. Recent research indicates that copper can compete with iron for the same binding sites in iron-sulfur clusters, thus affecting the assembly of [4Fe-4S] iron-sulfur clusters[27]. To investigate the impact of decreased copper uptake on iron-sulfur cluster formation in *M. smegmatis*, the study evaluated two groups of genes involved in this process. The first group, represented by the IscSUA-HscBA-Fdx gene cluster, serves a housekeeping function under normal

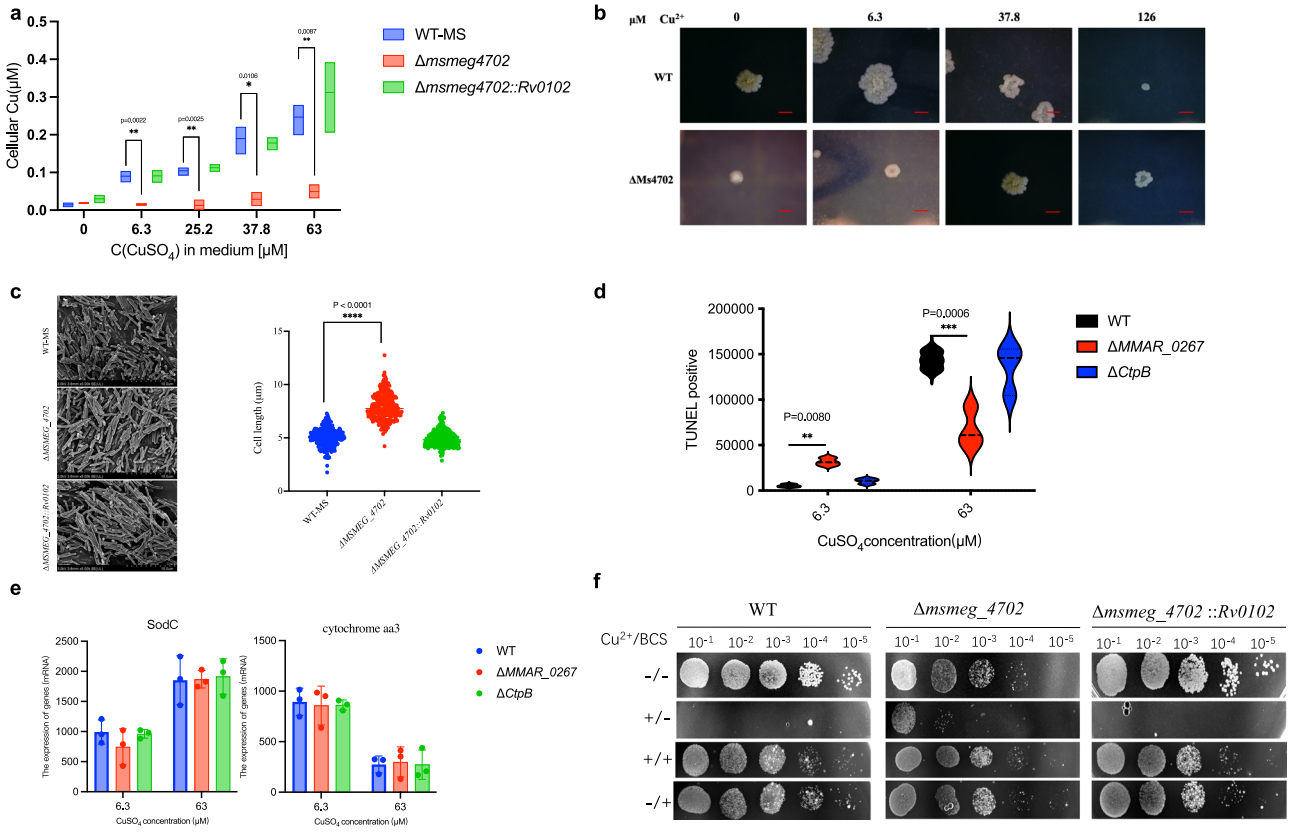

Fig. 3 | The intracellular copper ion level of MSMEG_4702 defective strain is lower than that of the wild type strain. a *M. smegmatis* (black bars), Δ*MSMEG_4702* (white bars), and *Rv0102* complemented strain (gray bars) were cultured in self-made Middlebrook 7H9 medium with 0, 6.3, 25,2, 37,8 63 μmol/L $CuSO_4$. Copper concentration was determined by measuring Cu (II)–Cuprizone complex absorption at 580 nm after 36 h of growth. Statistical significance: $^*P \le 0.05$, $^{**}P \le 0.01$, $^{***}P \le 0.001$; $n = 5$. Error bars represent standard deviation. **b** *M. smegmatis* WT and Δ*MSMEG_4702* were plated on 7H10 agar supplemented with various copper sulfate concentrations and incubated for 9 days at 37 °C. Representative colony pictures were taken using a stereomicroscope. **c** WT-MS, ΔMSMEG_4702 and Rv0102 complemented with 6.3 μmol/L $CuSO_4$ were processed for SEM, and morphologies were observed at 10,000 × cell lengths for 266 cells/samples were measured using Image J software and plotted as a scattered plot using GraphPad Prism9. Scale bars, 5 μm. **d** DNA damage levels at normal copper ion concentration (6.3 μM $CuSO_4$) and high copper concentration (63 μM $CuSO_4$) were measured by DNA damage kit ($n = 3$). **e** Investigation was conducted on the expression of two copper-requiring enzymes, copper-zinc superoxide dismutase SodC (MMAR_0747) and cytochrome c oxidase cytochrome aa3 (MMAR_1651), in *M. marinae* under both normal (6.3 μM $CuSO_4$) and high copper (63 μM $CuSO_4$) conditions ($n = 3$). **f** Serial dilutions of *M. smegmatis*, Δ*MSMEG_4702*, and Δ*MSMEG_4702::Rv0102* were plated on 7H10 plates with $CuSO_4$ and bathocuproine disulfonate (BCS). Plates were incubated at 37 °C for 4 days.

conditions, while the second group, encoded by the *Suf*ABCDSE gene cluster, functions as an alternative pathway for adapting to adverse environments such as iron starvation and oxidative stress[28]. Deletion of *MMAR_0267* noticeably decreased the expression of *Suf*A, *Suf*B, *Suf*C, and *Nif*U in the alternative housekeeping genes (Supplementary Fig. 5B), indicated that the formation of iron-sulfur clusters remained intact and oxidative stress was mitigated. Analysis of the transcription of *Isc*S and *Suf*A in 7H9 media containing 0–63 μM $CuSO_4$ showed minimal impact on the expression levels of *Isc*S by copper, with no significant difference between the wild-type and Δ*MSMEG_4702* strains (Supplementary Fig. 5C). As the $CuSO_4$ concentration increased, the transcription of *Suf*A also increased, with the wild-type strain consistently exhibiting higher *Suf*A levels than the Δ*MSMEG_4702* strain (Supplementary Fig. 5D). This suggests that copper exerts an inhibitory effect on iron-sulfur cluster synthesis, and the deletion of the *MSMEG_4702* gene can mitigate this effect, thereby reducing damage to iron-sulfur clusters within the cells and providing protective effects. Finally, AcnA activity, an indicator of iron-sulfur cluster activity[24], was found to be more affected by the addition of $CuSO_4$ in WT strains, indicating that the absence of MSMEG_4702 prevents the destruction of iron-sulfur clusters caused by high copper ion concentration (Supplementary Fig. 5E and 5F).

Bathocuproine (BCS) is a bidentate copper chelator known to form a 1:2 tetrahedral complex with monovalent copper ions (CuI), effectively removing CuI from the medium. The supplementation of BCS restored the growth of wild-type (WT) M. smegmatis under high copper concentrations (Fig. 3f). When added to a copper-free medium, BCS reduced copper utilization by *M. smegmatis*, leading to decreased growth (Supplementary Fig. 6A). To further investigate the copper specificity of the MSMEG_4702 protein, $CuSO_4$, AgNO3, FeCl3, Zn(CH3COO)2, and MnCl2 were added to the culture medium, and the growth of the ΔMSMEG_4702 mutant strain was measured. As the concentration of $CuSO_4$ increased, the growth of WT and ΔMSMEG_4702 strains gradually diverged, which is consistent with previous results showing similar growth at 36 μM copper concentration (Supplementary Fig. 6B). AgNO3, FeCl3, Zn(CH3COO)2, and MnCl2 had no effect on the growth ratio between WT and ΔMSMEG_4702 at different concentrations. These findings suggest that MSMEG_4702 specifically contributes to copper uptake during the growth of M. smegmatis and is not involved in the uptake of silver, iron, zinc, and manganese ions.

MMAR_0267 deletion enables *M. marinum* to inhibit mycobacteria-induced macrophage apoptosis by interfering with phagolysosome acidification

Mtb and other pathogens like it, rely on host nutrients, especially transition metals such as copper, iron, zinc, and manganese, for their virulence and growth[3]. Specifically, under conditions within a host's phagosomes, these pathogens might enhance their virulence by accelerating the uptake of

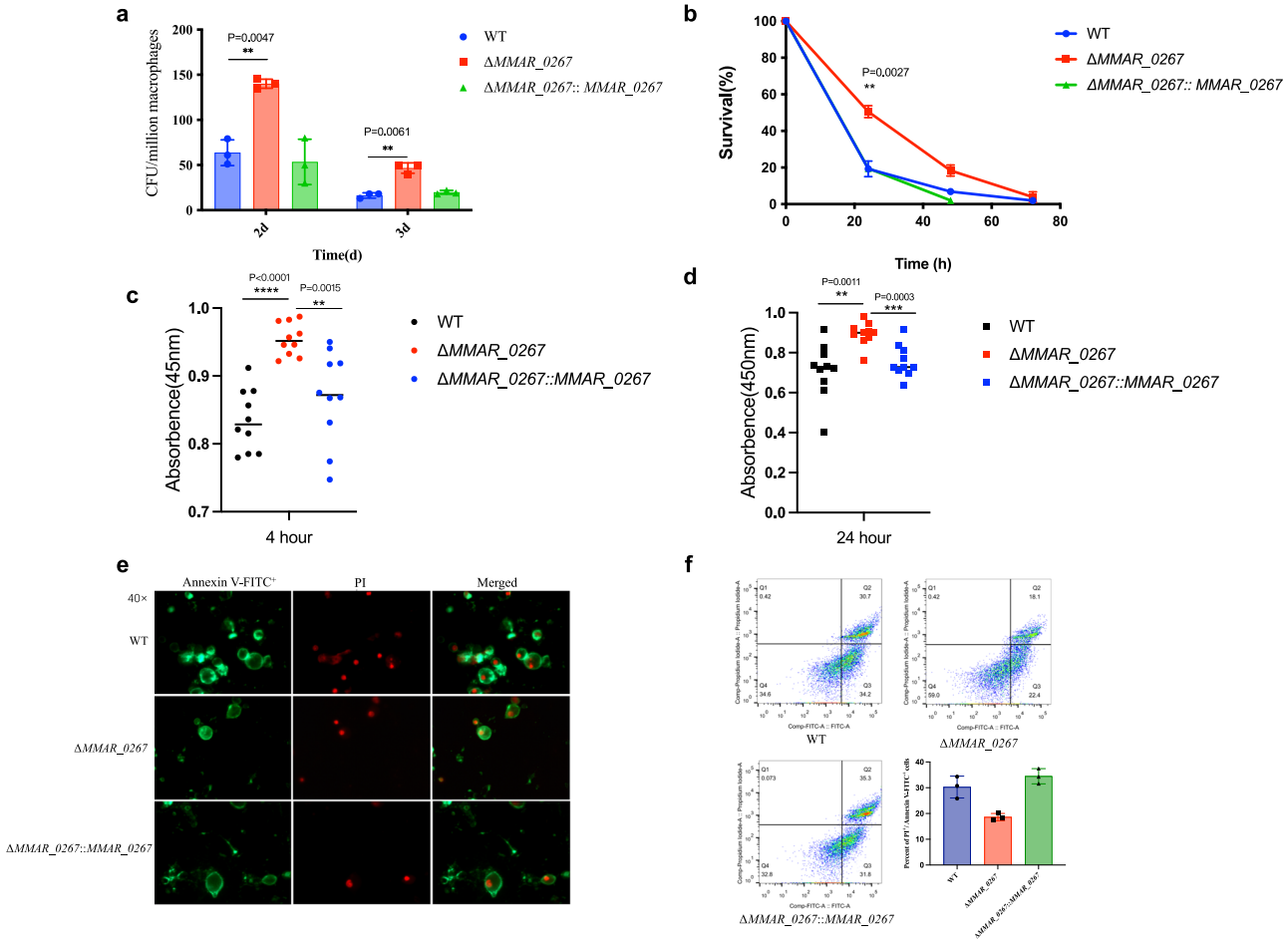

Fig. 4 | Δ*MMAR_0267* enhances the survival of *M. marinum* within macrophages and inhibits cell apoptosis. a THP-1 cells were infected with WT-*Mm*, Δ*MMAR_0267*, and Δ*MMAR_0267::MMAR_0267* at a MOI of 10. Infected cells were lysed with 0.025% SDS at specified times. Error bars show standar d deviation; (*$P \le 0.05$, **$P \le 0.01$, ***$P \le 0.001$; $n = 5$). **b** PMA-differentiated THP-1 macrophages were infected with the same strains at MOI of 10. Bacterial numbers were detected by plating lysates on MB 7H10 medium after 6, 24, 48, and 72 h of infection ($n = 5$). **c** and **d** CCK8 assay was used to assess THP-1 cell death when infected with *M. marinum* ($n = 3$). **e** Apoptosis levels in macrophages infected with the strains for 24 h were detected using a fluorescence microscope. **f** Inhibition of apoptosis by Δ*MMAR_0267* was confirmed by Annexin V-FITC/PI double staining after 48 h exposure, with Q1-Q4 representing different cell states ($n = 6$).

metals such as copper[29]. We infected THP-1 cells, a human monocytic cell line serving as a macrophage substitute, with wild-type (WT) *M. marinum* and *MMAR_0267* knockout strain. Upon infection, we recorded the bacteria's survival within the macrophages by quantifying the viable (CFU or colony-forming units) bacteria that remain. The results showed that the Δ*MMAR_0267* strain exhibited a significantly higher survival rate within the THP-1 macrophages compared to the WT strain at the 2- and 3-day post-infection mark (Fig. 4a). Additionally, the cell population infected with Δ*MMAR_0267* had a notably delayed clearance by the host's immune cells (Fig. 4b). The explanation for the improved survival rate for ΔMMAR_0267 maybe that it violates the host cell's regulation of programmed cell death mechanisms, known as apoptosis, which are vital for the pathogenic survival and replication[30,31]. We examined this more closely using molecular and cellular techniques. At 4 h and 24 h after infection, a cell viability assay indicated that Δ*MMAR_0267*-infected THP-1 cells had a significantly higher count of viable cells versus those infected with the WT and the complemented strain (Fig. 4c and Fig. 4d), suggesting that Δ*MMAR_0267* inhibited the occurrence of programmed cell death.

To substantiate the impact of Δ*MMAR_0267* on host cell survival and apoptosis prevention, we conducted comprehensive experiments using THP-1 cells, employing both fluorescence microscopy and flow cytometry to observe cells infected with pathogen strains. The Δ*MMAR_0267* showed a marked reduction in THP-1 cell apoptosis compared to the wild type (Fig. 4e-fluorescence microscopy, Fig. 4f-flow cytometry). We investigated the roles of MMAR_0267 and CtpB proteins in copper absorption and apoptosis inhibition in THP-1 cells. Both ΔMMAR_0267 and ΔCtpB strains exhibited apoptosis inhibition, indicating a shared impact linked to copper uptake deficiency (Supplementary Fig. 7A). Our exploration into MMAR_0267 overexpression aimed to determine if it would lead to excessive copper uptake and promote apoptosis. Contrary to expectations, overexpression did not significantly augment the growth or activity of *M. marinum* (Supplementary Fig. 7B and 7C), likely due to the intricate nature of the bacterial copper uptake pathway involving multiple proteins. Remarkably, MMAR_0267 overexpression also failed to induce apoptosis (Supplementary Fig. 7D), this suggests that MMAR_0267's role in apoptosis inhibition in THP-1 cells may be attributed to its modulation of copper sensitivity, thereby bolstering cell survival rates. This survival advantage potentially enables knockout strains to persist and secrete more virulence proteins such as CFP-10, which we subsequently identified. These virulence factors exert potent effects on the host, including apoptosis inhibition to evade host clearance. Additionally, there was no notable change in pro-inflammatory cytokine production (IL-1β, IL-10, and TNF-α) in THP-1 cells infected with Δ*MMAR_0267* (Supplementary Fig. 8), supporting that its enhanced viability in macrophages likely stems from apoptosis inhibition rather than direct inflammatory modulation.

Moreover, Δ*MMAR_0267* down-regulated apoptosis-promoting proteins BAX, P53, and Cas9, while up-regulating the anti-apoptotic protein Bcl2 (Fig. 5a), further confirming its ability to inhibit host cell apoptosis.

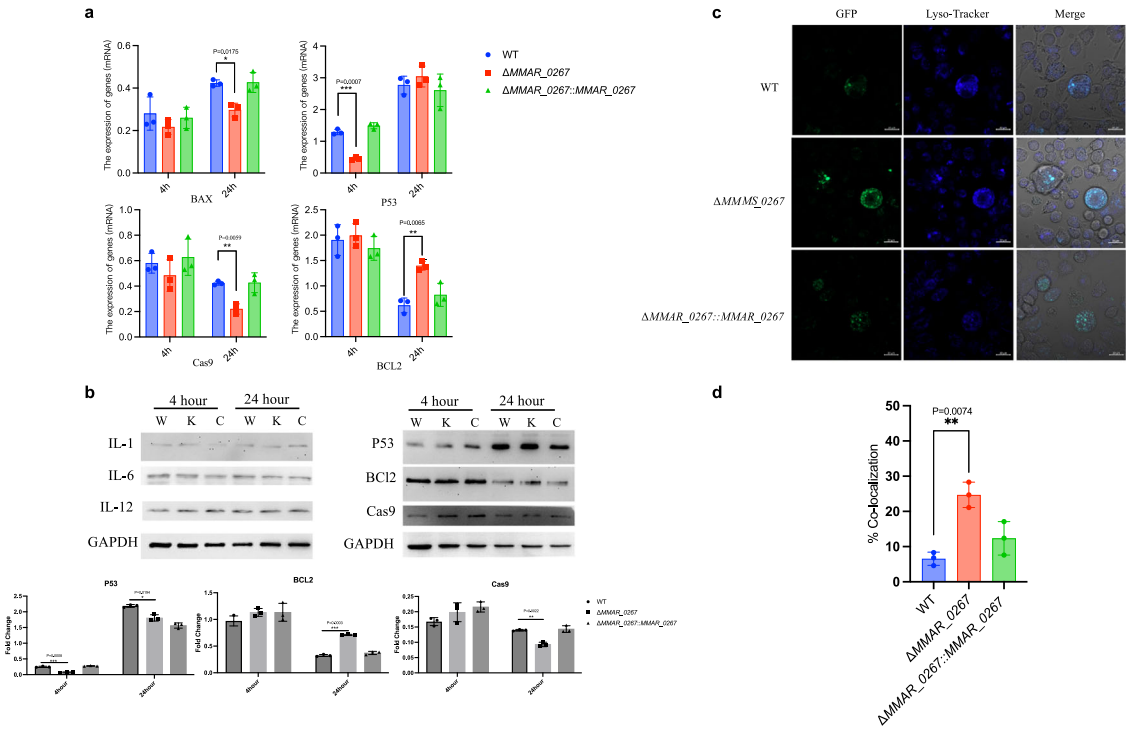

Fig. 5 | Deletion of *MMAR_0267* inhibited the level of apoptosis. a THP-1 cell RNA was extracted to measure the expression levels of cytokines P53, BCL2, Cas9, and BAX. Error bars represent standard deviation; (*$P \le 0.05$, **$P \le 0.01$, ***$P \le 0.001$; $n = 3$). **b** Immunoblotting was used to detect apoptosis-related molecules in THP-1 macrophages. Protein quantification of P53, BCL2, and Cas9 was conducted using ImageJ software. Western blot results were based on three replicates with triplicate samples for each condition. Grayscale analysis was utilized for quantification and statistical analysis ($n = 3$). **c** THP-1 macrophages were infected with WT-*MM*, Δ*MMAR_0267*, and Δ*MMAR_0267::MMAR_0267* strains labeled with GFP at an MOI of 20:1. Co-localization was analyzed using confocal immunofluorescence microscopy with LysoTracker-Blue DND staining. Representative images show saphirine representing co-localization of fluorescent signals. Scale bars are 20 μm. **d** Quantification of bacterial co-localization with LysoTracker DND blue. Mean values ± 1 s.e. depict the percentage of bacteria co-localizing with the LysoTracker signal in ~100 random cells, analyzed in a blinded fashion. Statistical significance: *$P < 0.05$, **$P < 0.01$ for WT-*MM*, Δ*MMAR_0267*, and Δ*MMAR_0267::MMAR_0267* (two-tailed Student *T* test).

Immunoblotting analysis indicated no significant differences in IL-1, IL-6, and IL-12 levels among THP-1 cells infected with Δ*MMAR_0267*, WT, and the complemented strain, but showed decreased P53 and Cas9 levels 24 h post-infection (Fig. 5b). These findings underscore that Δ*MMAR_0267* enhances *M. marinum*'s intracellular survival by primarily suppressing macrophage programmed cell death, rather than altering pro-inflammatory cytokine expression.

Apoptosis induction is typically beneficial for host defense against *Mtb* by enhancing mycobacterial cell killing and host protection[32]. The observed apoptosis suppression by Δ*MMAR_0267* suggests potential increased virulence, aiding evasion of innate immune defenses. *Mtb* infection often leads to membrane damage and necrosis induction, with lysosome-mediated membrane repair pathways crucial for *Mtb* survival[33]. Investigation into whether Δ*MMAR_0267* inhibits lysosomal acidification and lysosomal membrane permeabilization (LMP) revealed increased Δ*MMAR_0267* co-localization with lysosomes compared to WT, while the complemented strain showed normal lysosomal co-localization (Fig. 5c and Fig. 5d). These findings suggest that Δ*MMAR_0267* infection enhances lysosome fusion but inhibits LMP, potentially interfering with normal phagolysosome acidification processes.

MMAR_0267 deficiency increases zebrafish mortality upon *M. marinum* infection

To investigate the impact of reduced copper utilization on *M. marinum* virulence in zebrafish, we intraperitoneally infected thirty healthy adult wild-type zebrafish with 10 μl of 2 * 10^5 CFU/mL of either wild-type *M. marinum*, Δ*MMAR_0267*, or *MMAR_0267* complemented strains. Zebrafish infected with wild-type *M. marinum* succumbed on the 7th day post-infection, whereas those infected with Δ*MMAR_0267* died much earlier, by the 3rd day. Notably, all zebrafish in the Δ*MMAR_0267* infection group died 11 days earlier than those in the wild-type infection group (Fig. 6a). These results suggest that the deletion of *MMAR_0267* can enhance the virulence of *M. marinum*. Longitudinal survival analysis involved infecting zebrafish with the three strains and dissecting all infected fish on the 3rd day. The data showed that Δ*MMAR_0267*-infected zebrafish exhibited more severe symptoms of congestion, bleeding, and ulcers compared to those infected with the wild-type and complemented strains (Fig. 6b). CFU analysis of zebrafish tissues on the 3d day post-infection revealed significantly higher bacterial loads of Δ*MMAR_0267* in the liver and skin (Fig. 6c). Histopathological examination demonstrated increased neutrophil infiltration and necrotic areas in the liver and skin of zebrafish infected with Δ*MMAR_0267*, compared to those infected with the wild-type or complemented strains (Fig. 6d). These findings suggest that reduced copper utilization facilitates *M. marinum*'s resistance to the host's innate immunity, enhancing its intracellular growth and virulence during infection.

MMAR_0267 deficiency enables *M. marinum* to escape host immunity by dampening the macrophage STING-TBK1-IRF3 signaling

Deletion of the *MMAR_0267* gene in *M. marinum* extends its survival within the host, potentially leading to increased secretion of virulence proteins by the mutant strain. These proteins interact with the host, inducing significant changes that augment the pathogen's ability to evade the host immune system. Comprehensive transcriptomic and metabolomic analyses were conducted to gain further insights into the underlying mechanism by which *M. marinum* Δ*MMAR_0267* mutants enhance their toxicity towards zebrafish. Gene Set Enrichment Analysis (GSEA) of the transcriptome revealed that Δ*MMAR_0267* activation led to upregulation of

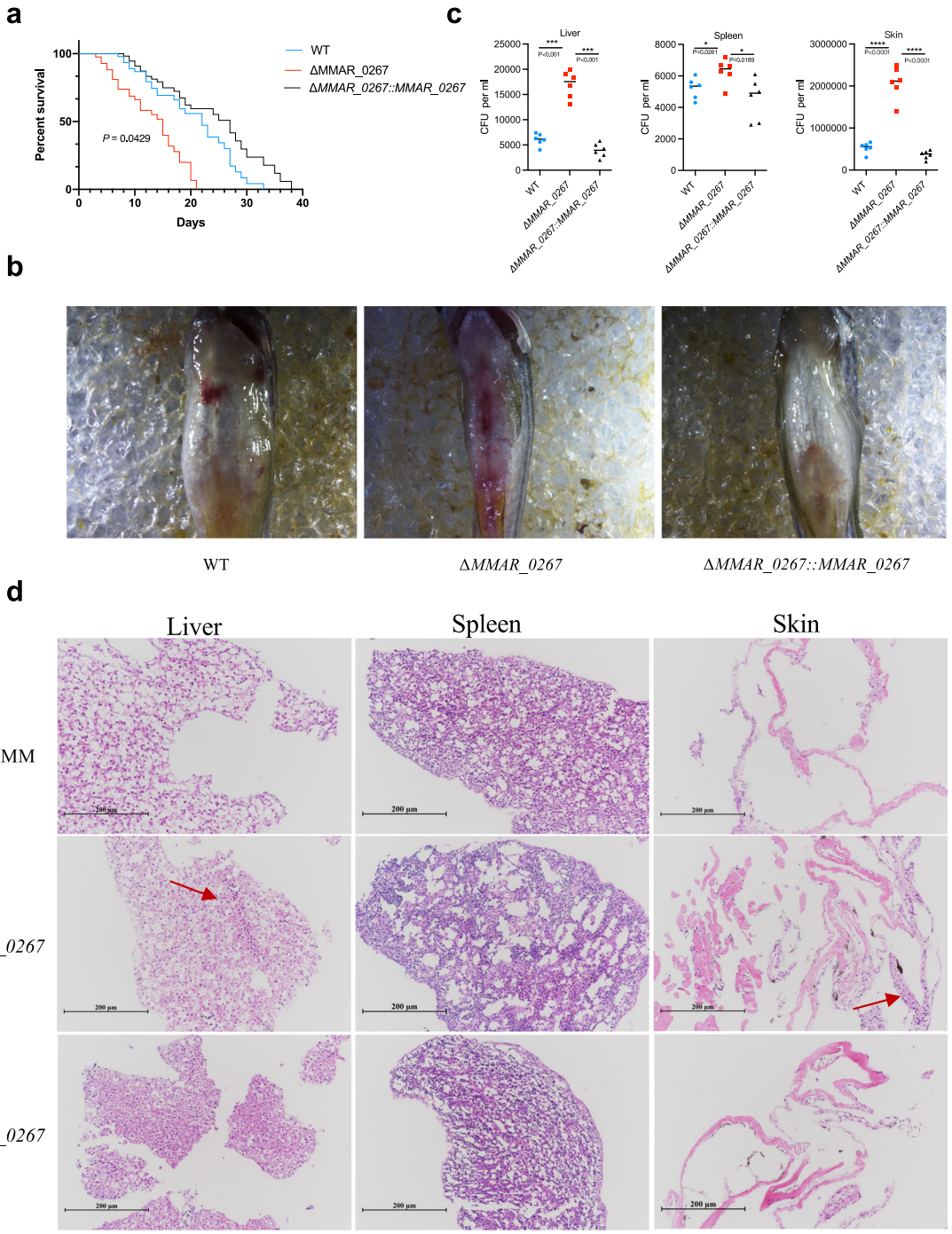

Fig. 6 | Deletion of *MMAR_0267* enhances the virulence of early *M. marinum* infection in zebrafish. a Survival of Zebrafish following *M. marinum* infection, representative of two independent survival studies ($n = 30$ fish/group). **b** Adult wild-type zebrafish were infected with WT, Δ*MMAR_0267* and Δ*MMAR_0267*::*MMAR_0267*, respectively. Each strain was adjusted to $OD_{600} = 0.5$, then 10 microliters were injected into the abdomen of zebrafish, and infection was photographed 3 days later. **c** Pathogenic behaviour of Δ*MMAR_0267* in infection models. Bacteria load quantification of liver/spleen and skin from 6 randomly chosen surviving zebra fish from each strain at day 3 after infection using CFU estimation method ($n = 3$). **d** H&E staining of representative infected liver/spleen and skin sections at 3 days post *M.marinum* -infection. Arrows indicate area of neutrophil infiltration with necrosis (scale bar = 200 μmol/L).

zebrafish pathways including glycolysis/gluconeogenesis, RIG-I-like receptor signaling, mTOR signaling, and IgA immune signaling (Fig. 7a). Heat maps of the transcriptome showed varying levels of differential gene expression related to the mTOR signaling pathway (TBK1, IRF3, etc.) in zebrafish infected with Δ*MMAR_0267 M. marinum* (Fig. 7b). Metabolomic analysis identified elevated levels of mTOR pathway-related metabolites (L-Arginine, L-Leucine, etc.) in the Δ*MMAR_0267* infection group. Additionally, there was an increase in alpha-ketoglutarate and a decrease in lactate, contrary to the typical glycolytic pathway, suggesting enhanced conversion of pyruvate to acetyl-CoA, thereby promoting the tricarboxylic acid cycle (Supplementary Fig. 9). The results obtained from the omics analysis demonstrate the activation of mTOR signaling played a crucial role in this process, as (1) mTOR complex 1 (mTORC1) can enhance the mitochondrial energy metabolism of infected macrophages through glycolysis to protect them from mycobacteria-induced death[34,35], (2) the mTOR signaling is regulated by early secreted antigenic target 6 (ESAT6) upon

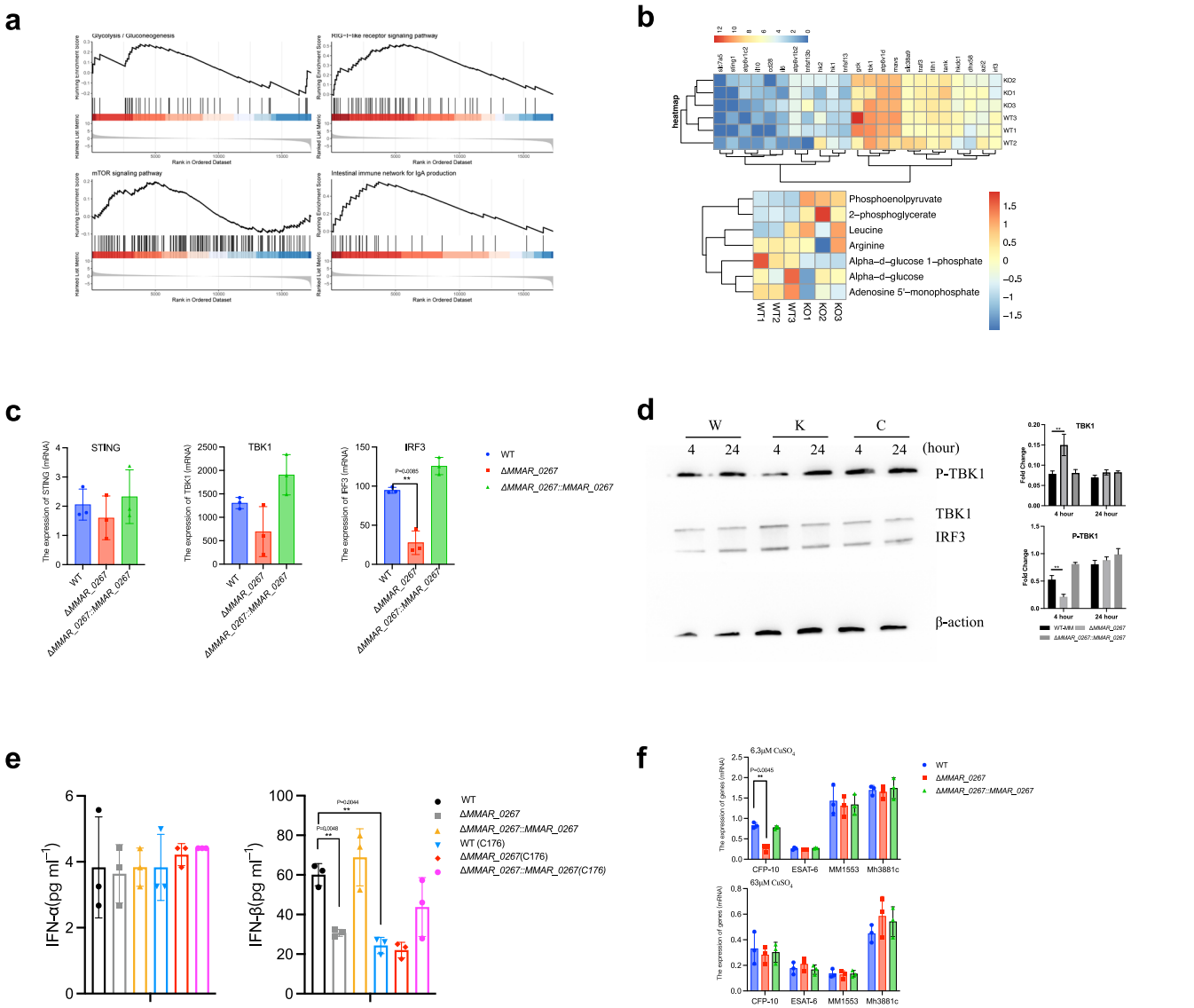

Fig. 7 | CFP-10 promotes STING-TBK1-IRF3 activation and inhibits cell apoptosis. a GSEA analysis was performed on the transcriptome of zebrafish infected with WT, Δ*MMAR_0267*, and Δ*MMAR_0267::MMAR_0267* strains. **b** Heat maps show related genes in glycolytic/gluconeogenesis pathways, RIG-I-like receptor signaling pathways, mTOR signaling pathways, and IgA immune signaling pathways, along with metabolomic heat maps of their signature products. Both transcriptome and metabolomic analysis were conducted on zebrafish infected with WT and Δ*MMAR_0267* strains, each with three replicates. **c** The Δ*MMAR_0267* mutant strain reduced the transcription of TBK1 and IRF3 in THP-1 cells infected with different strains. Gene expression levels were quantified by detecting STING, TBK1, and IRF3 transcripts, normalized to the internal reference gene SigA. Data represent average mRNA abundances from cells cultured in triplicates ($n = 3$). **d** TBK1 and phosphorylated TBK1 expression in THP-1 cells at 4- or 24 h post-infection were analyzed by Western blotting. Protein quantification was done using Image J software. **e** ELISA was used to quantitatively detect IFN-α and IFN-β levels in the liver of zebrafish infected with different strains ($n = 6$). **f** Transcription of CFP-10 in different strains at varying $CuSO_4$ concentrations was measured using RT-qPCR ($n = 3$).

Bacillus Calmette-Guérin (BCG) vaccination[36]. Previous studies have demonstrated that the activation of TBK1 can inhibit the activity of mTORC1, leading to suppressed protein synthesis and enhanced autophagy[37]. The phosphorylation level of STING-TBK1-IRF3 has been shown to impact the activation of the mTOR signaling pathway. In line with this hypothesis, quantitative real-time PCR (qRT-PCR) analysis revealed a significant decrease in the mRNA levels of TBK1 and IRF3 in zebrafish infected with Δ*MMAR_0267 M. marinum* (Fig. 7c), suggesting that the inhibition of apoptosis is occurring, thereby potentially enhancing the survival of the bacteria within infected macrophages. We observed a noteworthy reduction in phosphorylated TBK1 in THP-1 cells during early infection with Δ*MMAR_0267 M. marinum* (Fig. 7d). This finding indicates that the STING-TBK1-IRF3 axis may directly modulate the mTOR signaling pathway. Activation of the STING-TBK1-IRF3 axis has been linked to the production of type I interferons (IFN-α/β) and promote cell apoptosis[38,39]. Our findings demonstrated a notable decrease in the levels of IFN-β in THP-1 cells infected with *MMAR_0267*-deficient *M. marinum*, and this reduction was further inhibited by C176 (a potent and covalent STING inhibitor), while IFN-α showed no significant changes (Fig. 7e). This suggested that Δ*MMAR_0267 M. marinum* primarily enhances its virulence by suppressing the expression of host type I interferon IFN-β through inhibition of the STING-TBK1-IRF3 axis, possibly by modulating the phosphorylation of TBK1. Additionally, we have observed significant activation of the mTOR signaling pathway. Previous studies have shown that the secreted effectors of the *Mtb* ESAT-6 secretion system-1 (ESX-1) can regulate the mTOR signaling in infected cells. Hence, we aimed to elucidate

which effector among the four secreted antigens (CFP-10, ESAT-6, MM1553, and Mh3881c) of Esx-1 substrates is involved in this process[40]. We observed a significant reduction in the expression of the CFP-10 antigen in *MMAR_0267*-deficient *M. marinum* under normal copper conditions (6.3 μmol/L), while this expression was increased when copper levels were elevated (63 μmol/L) (Fig. 7f). Indicating that the Esx-1 secretion system may be involved in the inhibition of the STING-TBK1-IRF3 axis. To further investigate this, a double knockout strain of *MSMEG_4702* and CFP-10 was constructed and employed it for infecting THP-1 macrophages. Following treatment with 63 μmol/L $CuSO_4$, only the Δ*MSMEG_4702 M. marinum* strain exhibited an increase in TBK1 phosphorylation, while the double knockout strain showed no effect on TBK1 phosphorylation (Supplementary Fig. 10). These findings collectively indicate that *MMAR_0267* deletion in *M. marinum* enhances virulence through complex interactions involving mTOR signaling activation and modulation of host immune responses via the STING-TBK1-IRF3 axis, potentially facilitated by ESX-1 effectors like CFP-10.

Discussion

Copper is an essential trace metal in bacteria and serves as a cofactor for many enzymes, but it can be lethal at high concentrations. Multiple studies have shown that copper can rapidly and effectively kill various pathogenic bacteria, including *Escherichia coli*, *Staphylococcus aureus*, *Clostridium difficile*, *Salmonella*, *Mycobacterium*, *Faecalis*, and *Enterococcus aureus*[18]. In fact, high concentrations of copper were found in guinea pig granulomas during *Mtb* infection[29]. Subsequent investigations unveiled that mycobacterial phagosomes have the ability to accumulate high concentrations of copper during Mtb infection, which could serve as a potential defense mechanism against the pathogen[41]. In this study, we have identified a novel protein, MMAR_0267 (Homologous protein of Rv0102), that plays a crucial role in the utilization of copper ions in mycobacteria. While it has been previously discovered that the outer membrane pore protein family, *Msp*A, *Msp*B, and *Msp*C, are involved in copper uptake in *M. smegmatis*, the Msp family homologs are absent in *Mtb*[42], and it remains unclear how copper enters *Mtb* cytoplasm.

Secondary structure analysis has revealed the presence of two significant domains in Rv0102 (Fig. 1e). The first domain is the CopD domain, which is responsible for the uptake of copper from the periplasm to the cytoplasm[43]. Despite the absence of the Cop family in *Mtb*, the presence of the functional CopD domain in Rv0102 implies its potential involvement in a similar role within mycobacteria. This hypothesis is substantiated by the observation that the Δ*MSMEG_4702* strain exhibited viability in culture medium containing 100 μmol/L $CuSO_4$ (Fig. 2d). Although the deletion of *MSMEG_4702* did not entirely impede copper utilization by mycobacteria, the knockout strain displayed growth defects with the gradual increase in $CuSO_4$ concentration in the medium, presumably due to copper overload (Fig. 2). These results imply that the pathway for copper uptake in mycobacteria is not exclusive and that under conditions of abundant copper, non-specific uptake pathways may be activated. Additionally, a recent study has proposed the involvement of *Mtb* P-type ATPase CtpB in copper uptake[6]. The second domain in Rv0102 is the cytochrome Caa3 domain, which incorporates a copper-binding center capable of binding CuA, CuI, and CuII in a mixed-valence state[44]. Bioinformatic analysis indicates that Rv0102 can both bind to copper and transport the bound copper to the cytoplasm. Moreover, the experimental data demonstrate a noticeable disparity in the intracellular copper ion content between WT and Δ*MSMEG_4702*, even under identical growth conditions (Fig. 3a). This discrepancy can be attributed to the enhanced capability of the knockout strain to efficiently utilize copper at higher concentrations, thereby facilitating its growth. Conversely, the wild-type strain experienced growth inhibition due to heightened copper toxicity. These findings unveil a novel factor that governs the growth and development of *M. smegmatis*, particularly highlighting the role of copper.

The tolerance of Δ*MMAR_0267* to high concentrations of copper may contribute to its survival within the macrophage's phagosomes. Our findings revealed that the infection of Δ*MMAR_0267* inhibited the apoptosis of THP-1 cells and enhanced its intracellular survival. The regulatory mechanisms of cell death encompass apoptosis, ferroptosis, necrosis, and the newly discovered cuproptosis[45]. Immunoblotting of various death-critical molecules indicated a decrease in the levels of P53 and Cas9, which are known to promote apoptosis (Fig. 5b). The observed inhibition of apoptosis may be attributed to copper tolerance, as the deletion of CtpB, responsible for copper intake, also results in the inhibition of apoptosis. Additionally, in the natural host of *M. marinum*, zebrafish, our observations revealed that zebrafish infected with the knockout strain exhibited a mortality rate 4 days earlier than those infected with the WT strain (Fig. 6a), and histological analysis of tissue sections exhibited more pronounced liver damage in the knockout group (Fig. 6d). CFP-10 associates with secreted proteins, including ESAT-6 and CAML (calcium-modulator and cyclophilin ligand), forming a complex on the host cell membrane, facilitating its entry of the bacterium into the host cell and triggers apoptosis and inflammatory responses, thereby exhibiting its virulence[46]. Our results indicate that copper ions may enhance the transcription of the CFP-10 virulence factor in *M. marinum*. However, it remains unclear whether copper directly regulates cell apoptosis. The findings suggest that the two factors function independently. Notably, we observed no significant changes in the transcription levels of *MMAR_0267* and *Ctp*B, two genes involved in copper utilization, when the copper concentration in the medium was increased. In contrast, the transcription of *Ctp*V, which is involved in copper efflux, was upregulated (Supplementary Fig. 11). These findings suggest that *M. marinum* employs a strategy of increasing copper storage and efflux to counteract the toxicity of high copper levels within cells, rather than reducing copper uptake. It is worth noting that there exists a delicate balance between mycobacterial infection and the level of host cell apoptosis[47]. In the case of Δ*MMAR_0267* infection, the phenomenon of bacterial inhibition of apoptosis may be further amplified due to its copper tolerance and enhanced survival.

The discovery of MMAR_0267 as a copper transport protein provides valuable insights into the mechanisms underlying the acquisition and utilization of copper by *Mtb*. This finding, illustrated in Fig. 8, offers important information for enhancing our understanding of copper metabolism in *Mtb*. In conclusion, our findings indicate that the absence of *MMAR_0267* in *M. marinum* triggers the activation of host glycolysis, mTOR signaling, and the suppression of apoptosis, ultimately enhancing bacterial survival within infected macrophages and increasing virulence in zebrafish. This study highlights the significance of comprehending the molecular mechanisms involved in bacterial pathogenesis and host immune responses, which can contribute to the development of novel and effective treatments.

Methods

Bacterial strains and culture conditions

M. smegmatis mc^2 155, X674 and complemented strains were grown in Middlebrooks 7H9 medium supplemented with 0.05% Tween 80 and 0.2% glycerin. Solid medium is 7H10-Dubos oleic acid complex-glycerol agar. Selected antibiotics were used at indicated concentrations: kanamycin, 50 μg/mL; ampicillin, 100 μg/mL for *E. coli* and 20 μg/mL for *M. smegmatis* mc^2 155; hygromycin, 100 μg/mL for *E. coli* and 50 μg/mL for *M. smegmatis* mc^2 155 at 37 °C with shaking. *M. marinum* was cultured using the same antibiotic concentration but under constant temperature of 30 °C.

Construction and screening of *M. smegmatis* mc^2 155 Φ MycoMar insertion library

The ΦMycoMarT7 transposon system was utilized to construct a transposon insertion mutant library of *M. smegmatis* mc^2 155 as previously described[48]. The ΦMycoMarT7 transposon system was used to create a transposon insertion mutant library of *M. smegmatis* mc^2 155. The donor strain was grown in Middlebrook7H9 broth with 10% OADC at 37 °C until reaching an OD_{600} of 0.6-0.8. The phage carrying the transposon sequence was then transferred to the recipient strain at a 1:1 ratio by electroporation. Transposed cells were plated on Middlebrook7H10 agar with 10% OADC and

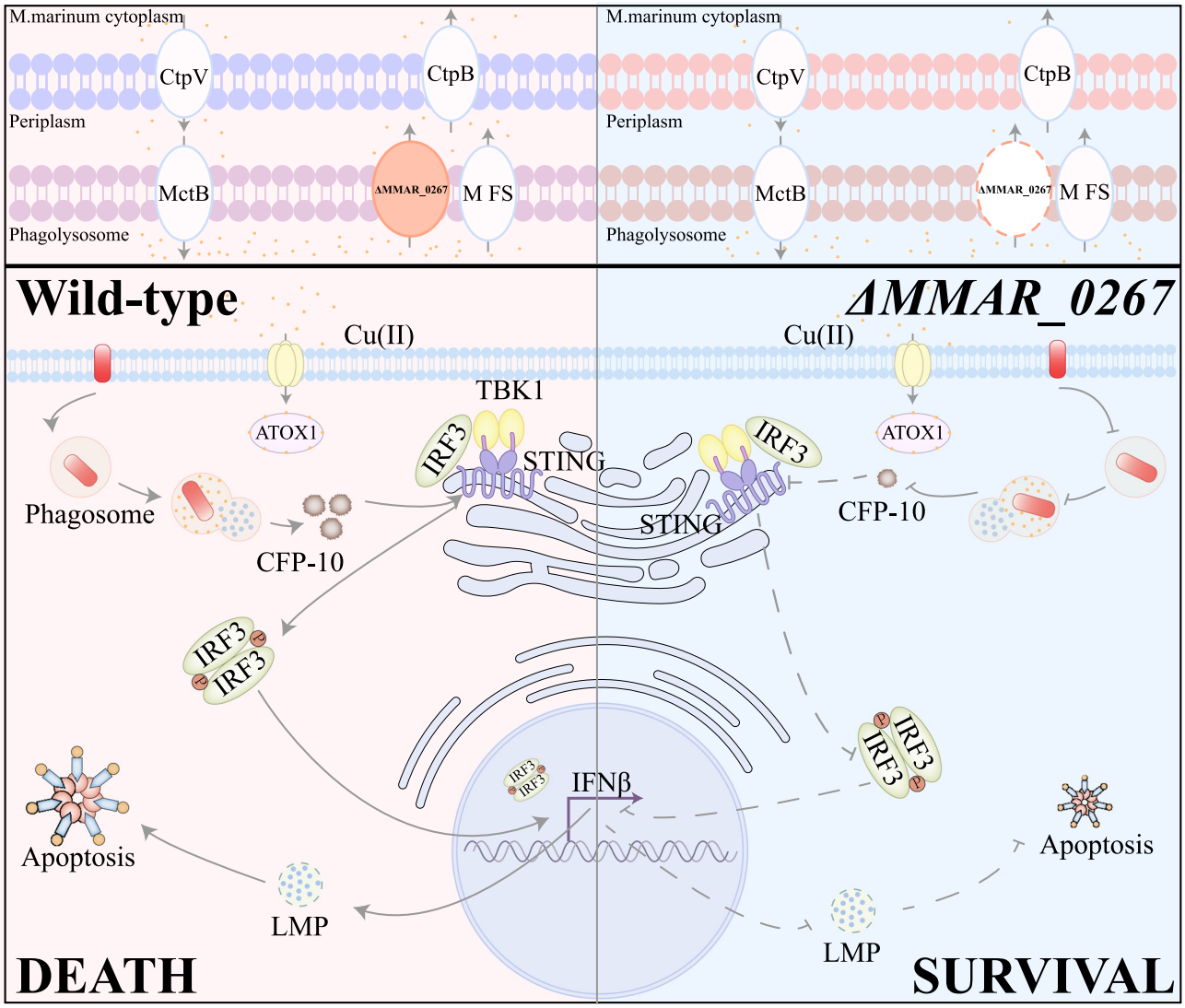

Fig. 8 | Bactericidal effect of copper in macrophages and the role of MMAR_0267 in copper homeostasis. In macrophages, copper ions are absorbed using the high-affinity Cu transporter Ctr1 when engulfing *M. marinum*, then transported to Atp7A via Atox1, and finally transferred into the phagosome by Atp7A to create a bactericidal environment rich in copper. To counter copper stress, MctB and CtpV are upregulated to excrete excess copper. MMAR_0267, as the copper uptake protein on the membrane, plays a crucial role in macrophage bactericidal activity. Deficiency of MMAR_0267 enhances the intracellular survival of *M. marinum* in the phagosome, while reducing secretion of the virulence factor CFP-10, leading to suppressed TBK1 phosphorylation and inhibited cellular apoptosis.

50 μg/mL kanamycin, and colonies were allowed to form at 37 °C for 2–3 days. For phage infection, *M. smegmatis* cells in late-log phase were washed and suspended in Mycobacteriophage buffer before adding phages at a 10:1 ratio and incubating at 37 °C for 4 h. The bacteria were then plated on Middlebrook7H10 agar with 20 μg/mL kanamycin and incubated for 3–4 days to obtain kanamycin-resistant colonies. These colonies were further plated on Middlebrook7H10 agar to create a library of 20,000 clones. Screening involved plating clones on Middlebrook7H10 agar with 20 μmol/L $CuSO_4$ to identify copper-tolerant strains. After screening, PCR sequencing and bioinformatics tools were used to analyze the identified genes.

Defining the insertion-disrupted gene of Φ MycoMar

The mutation library was screened in 7H9 containing 20 μmol/L $CuSO_4$. The high-efficiency thermal asymmetric interlaced PCR (hiTAIL-PCR) technique was employed to amplify the unknown flanking sequence from the mutant genome with transposon insertion. The specific primers used in this experiment are detailed below: TAIL-1(X): 5'-TGCTCCTGCCGAGAAAGTATC-3', TAIL-2(X): 5'-ACGATGGACTCCAGAGTCTTCTGAGCGGGACTCTGTA-3', TAIL-3(T): 5'-GCCTTCTTGACGAGTTCTTCTGAG-3', LAD1-1: 5'-ACGATGGACTCCAGAGCGGCCGCVNVNNNGGAA-3', LAD1-2: 5'-ACGATGGACTCCAGAGCGGCCGCBNBNNNGGTT-3', LAD1-3: 5'-ACGATGGACTCCAGAGCGGCCGVNVNNNCCAA-3', LAD1-4: 5'-ACGATGGACTCCAGAGCGGCCGBNBNNNCGGT-3', AC-1: 5'-ACGATGGACTCCAGAG-3'. The hiTAIL-PCR protocol was conducted according to the reference[49], and DNA recovery was performed using the Tiangen Company's DNA recovery kit. For TAIL-PCR products presenting a single band, direct recovery was conducted. In cases with multiple bands, the target band was excised for gel recovery. Following this, TAIL-PCR products were submitted to BGI Genomics Company for sequencing, with the sequencing primers being the upstream and downstream primers from this PCR round. Subsequently, the NCBI Blast function was utilized to compare the sequencing results with the complete genome of M. smegmatis, enabling the determination of the gene location of transposons.

Construction of the *M. smegmatis* deletion mutant in *MSMEG_4702*

The upstream and downstream homologous arm sequences of *MSMEG_4702* gene were obtained by amplification of KOF1(5′- CCGATTGGGAGCAGCAGG -3′), KOR1(5′- ATCACGCCGCTGACACCCCTACGCACGCACG

TCAGAGGC -3′), KOF2(5′- GCCTCTGACGTGCGTGCGTAGGGGTGT CAGCGGCGTGAT -3′) and KOR2(5′- CGCGAAGACCATGCCGATC -3′) primers from the genome of wild-type *M. smegmatis*, respectively. By overlapping PCR, they were merged into a single fragment and ligated to pDM19-T, which was named pDM19-T-MS. Using *Bgl* II enzymes to cut dif - hyg - dif box from the plasmid pAL75, ligated by the same enzyme used pDM19 - T - MS building to get the pDM19 - T - MS - hyg, *Bam*H I and *Spe* I enzymes were used, the recombinant fragments were amplified and transformed into the *M. smegmatis* competent cell with pJV53 plasmid by electrotransformation, then spread on the 7H10 plate with Kan and hyg to screen the deletion mutant, and then cultured in the absence of antibiotics 7H9 medium and transferred five generations to allow the loss of Hyg box and pJV53 plasmid. The *MMAR_0267* gene of *M. marinum* was knocked out by using the same method, with the primer sequence as follows: KOF1(5′- GCCCAAGCTTACATGACCGCCCAAA -3′), KOR1(5′- AGATCTCCCT CGAGCTTACGACTGGATGTCG -3′), KOF2(5′- CCAGTCGTAAGC TCGAGGGAGATCTAGGCGGGGACGGATCGCTAGCCGAC -3′) and KOR2(5′- TGGACGGTGAGGTCTTTGACGCTGT -3′).

Complementation with *Mtb Rv0102* gene and western blot

Mtb Rv0102 gene was amplified by PCR from *Mtb* H37Rv genome using the forward primer 5′- CGGGATCCATGGGGACGCACGG -3′and reverse primer 5′- CCATCGATTCAGCGCCGCATTCGCG -3′, digested using *Nde*I and *Cla*I restriction enzymes and ligated with pALACE plasmid (A *Mycobacterium* expression test plasmid as a gift from Professor Yossef Av-Gay, University of British Columbia, hygromycin resistance). Desired *E. coli* clones were screened on solid LB medium containing hygromycin. The recombinant plasmid was then transformed into mycobacterial cells by electroporation, empty pALACE plasmid subjected to the same procedure was used as a negative control. All transformants were selected by hygromycin (50 μg/mL) on Middlebrook 7H10 agar. Supplemented *M. smegmatis* strains were cultured in 50 mL Middlebrook 7H9 liquid medium to an OD_{600} of 0.8-1.0 in the presence of 50 μg /mL hygromycin. Bacteria were washed (three times) with ice-cold 1 × PBS, and then suspended in the same buffer. Sonication was used to lyse cells.100 μL total cell lysates were resolved on 12% SDS-PAGE, followed by Western blot analysis. Specific anti-Myc monoclonal antibody (TIANGEN, China) was detected with IgG-HRP, an anti-mouse IgG monoclonal antibody labeled with horseradish peroxidase (TIANGEN, China).

Growth curves

Growth curves for wild type and mutant *M. smegmatis* strains were assessed by spectrophotometry (UV-VIS spectrophotometer, Varian Cary 50). Briefly, overnight-cultured bacteria were diluted with liquid 7H9 to an optical density of 0.8. 1% inoculum was then transferred into a fresh liquid 7H9 without or with $CuSO_4$ of different concentrations. Samples were incubated at 37 °C at110 rpm/min. Optical density was determined every 4 h for consecutive 60 h.

Determination of copper accumulation

The copperprizone microplate method is used to quantify the copper content in *M. smegmatis*. copperprizone, a copper chelating agent, forms a blue copper ketone complex with copper ions. Its unique structure gives it high affinity and selectivity with copper ions, showing specificity in its reaction. Pre-cultured strains of WT, Δ*MSMEG_4702*, and Δ*MSMEG_4702::Rv0102* were inoculated into 7H9 medium with varying copper ion concentrations (0, 6.3, 25.2, 37.8, and 63 μmol/L) by adding $CuSO_4$. Each strain was incubated in triplicate in shaking flasks at 37 °C for 3 days. After centrifugation at 12,000 × g, 4 °C for 10 min, pellets were washed with metal-ion-free PBS. OD at 600 nm was adjusted to 1.0 using ddH_2O. Samples underwent sonication, lysis buffer addition, and centrifugation at 4 °C, 12,000 × g for 10 min. The supernatant was used for copper content determination with the Cell Copper (Cu) Colorimetric Assay Kit. Refer to the instructions provided for specific procedure steps.

For the heat-killed control group, pre-cultured strains were washed with metal-ion-free PBS and suspended in sterile deionized water. Bacterial suspension was heat treated at 100 °C for 20 min. After treatment, $CuSO_4$ solution was added to achieve copper ion concentrations of 0, 6.3, 25.2, 37.8, and 63 μmol/L. The mixture was incubated at 37 °C for 1 h and then washed with metal-ion-free PBS. OD_{600} was adjusted to 1.0, followed by sonication and copper ion quantification using the Cell Copper (copper) Colorimetric Assay Kit. Accumulated copper was determined by subtracting copper ions adsorbed in the heat-killed group from the total copper ions in the culture.

The detection method for zinc ions is similar to that of copper ions, but it employs the 5-Br-PADAP microplate method for determining zinc ion concentration. In this method, zinc ions in the sample form a colored complex with the 5-Br-PADAP reagent, and the intensity of the color is proportional to the concentration of zinc ions. All *M. smegmatis* strains were cultured using the same previously described method, but with different final concentrations of zinc ions (adding $ZnSO_4$): 0, 5, 10, 20, and 40 μmol/L. After incubating the bacteria, both the cultures and heat-killed cells were collected and subjected to ultrasonic treatment for cell lysis. The zinc content in the bacteria was then determined using the Zinc (Zn) Colorimetric Assay Kit.

Antibiotic susceptibility assays

For antibiotic susceptibility assays, *M. smegmatis* wild-type and mutant strains were grown to an OD_{600} = 0.8. The susceptibility to antibiotics was determined by spotting a 10-fold serially diluted samples on Middlebrook 7H10 (Difco) plates containing 0.05 μg/mL moxifloxacin. All experiments were repeated at least three times.

RNA isolation and real-time quantitative TaqMan PCR assay

A 50 mL bacterial culture with OD_{600} = 0.3 was diluted (1:100) into 7H9 media. The strains were cultured until OD_{600} = 0.8, then split into untreated (control) and treated groups. Cells in the treated group were exposed to 0.05 μg/mL moxifloxacin for 30 min, followed by centrifugation at 12,000 x g. Bacterial pellets were suspended in TRIzol (Invitrogen, USA) for RNA extraction and purification per the manufacturer's instructions. cDNA was synthesized using the Superscript III First-Strand Synthesis System kit (Invitrogen, USA). Quantitative real-time reverse transcription-PCR was conducted with cDNA from 50 ng RNA using an SYBR Green Supermix kit (Applied Biosystems) to assess gene expression. Expression levels were normalized to sigA as the control, and the relative expression means were averaged over three replicates.

Localization of the Rv0102 protein

M. smegmatis recombinant strains harboring the *Rv0102*- pALACE-myc and pALACE-myc empty vector were grown as previously described. The cells were lysed by sonication. Cell debris and intact cells were removed by centrifugation (3000 × *g*) for 5 min, and the supernatant was centrifuged (27,000 × *g*) for 30 min at 4 °C. The pellet contained cell wall, whereas the supernatant represented the cell membrane and cytosol fractions. The pellet and supernatant were used to detect the recombinant protein and GroEL2 (cytoplasmic protein control) by Western blotting with anti-Myc antibody and anti-His antibody.

Bacteria sample preparation for Scanning Electron Microscope (SEM) and Transmission Electron Microscope (TEM)

The bacterial solution was centrifuged at 8000 g for 10 min to remove the supernatant. The samples were fixed with 2.5% glutaraldehyde solution for 3 h, followed by resuspension in 1 × PBS buffer for 15 min. For SEM, the strains were dehydrated using a gradient of ethanol concentrations (50%, 70%, 80%, 90%, and 100%), and then resuspended in an ethanol and tert-butyl alcohol mixture (1:1) after snap-freezing and freezing-thawing for morphological observation under a microscope. For TEM, the strains were treated with 1% osmium tetroxide for 2 h, dehydrated with a gradient of ethanol and acetone concentrations, and embedded in epoxy resin for

ultrathin sectioning to observe the cell membrane of M. smegmatis under a transmission electron microscope.

In vitro infection with recombinant *M. marinum*

THP-1 cells were cultured in RPMI 1640 medium (Invitrogen) supplemented with 10% (v/v) heat-inactivated FBS, 2 mM L-glutamine, 100 μg/mL streptomycin, and 100 U/mL penicillin (Invitrogen) at 37 °C with 5% CO_2. Cells were seeded at 2×10^6 cells/well in 6-well plates and differentiated with 100 ng/mL PMA. After differentiation, cells were infected with WT, Δ*MMAR_0267* and Δ*MMAR_0267*:: *MMAR_0267 M. marinum* at an MOI of 10. Four h post-infection, cells were washed with PBS, and gentamicin (100 μg/mL) was used to eliminate extracellular bacteria. For LDH activity assay, culture supernatants were collected at 6, 24, 48, and 72 h post-infection and analyzed using a commercially available LDH cytotoxicity kit (Takara Bio). For intracellular bacterial survival, THP-1 cells were infected with the aforementioned strains for 6, 24, 48, and 72 h at 37 °C. Infected cells were washed three times with PBS, lysed in 1 mL of 0.025% SDS, diluted, and plated on 7H10 agar plates with 10% glycerol. After 3 days of incubation, colony-forming units were counted to calculate the survival rate compared to the control.

Zebrafish infection with *M. marinum*

WT, Δ*MMAR_0267* and Δ*MMAR_0267*:: *MMAR_0267 M. marinum* were grown on 7H10 plates, a single colony was picked for culture in liquid medium at 30 °C until the $OD_{600} = 0.5$. Healthy adult zebrafish was selected from a population and acclimated them in fresh water for 24 h before grouping. The *M. marinum* culture was centrifuged to remove the supernatant, the bacteria were washed with PBS three times, and diluted the bacterial suspension to 10^8 CFU/mL. The zebrafish was placed into a new dish, 10 μL bacterial suspension was injected into the zebrafish abdomen. After infection, the zebrafish was placed to the acclimation water. At different time points after infection, the fish was recorded for signs of illness and death. Simultaneously, the bacteria were isolated from dead fish to determine the species and count the bacterial load.

Metabolomics and transcriptomics of zebrafish

Mycobacterium marinum is cultured on 7H10 agar plates overnight, and single colonies are selected for propagation in liquid medium at 30 °C until reaching an optical density of ~0.5. Concurrently, healthy zebrafish embryos are raised to adulthood, acclimatized in fresh water for 24 h, and grouped. To initiate infection, the bacterial culture is centrifuged, washed with PBS, and then diluted to 10^8 CFU/mL. Zebrafish are abdominally injected with 10 μL of the bacterial suspension and returned to acclimatization water for 3 days. On the 3rd day post-infection, liver tissues are extracted from zebrafish for downstream analysis.

The liver samples are sent to APTBIO in Shanghai, China for transcriptome and metabolome analysis. For transcriptome analysis, high-purity RNA extraction from liver samples is essential to prevent RNA degradation. This process involves enriching mRNA with Oligo dT-coated magnetic beads, fragmenting the RNA, synthesizing cDNA using random hexamer primers, purifying the double-stranded cDNA, and preparing the cDNA library for sequencing after PCR enrichment. The resulting data undergoes bioinformatics analysis.

In metabolomics, after removing the sample at -80 °C, weigh 20 mg of the sample, add 50 μl of water MP, vortex for 60 s, add 200 μl of methanol-acetonitrile solution (1:1, v/v), vortex for 60 se, perform low-temperature sonication for 30 min twice, precipitate the protein by placing it at -20 °C for 1 h, centrifuge at 14000 rcf, 4 °C for 20 min, collect the supernatant for freeze-drying, and store the sample at -80 °C. The sample is separated using an Agilent 1290 Infinity LC Ultra High-Performance Liquid Chromatography System (UHPLC) with a HILIC column; the column temperature is maintained at 25 °C; the flow rate is 0.3 mL/min; the mobile phase consists of A: water with 25 mM ammonium acetate and 25 mM ammonia solution, and B: acetonitrile. The gradient elution program is as follows: 0–0.5 min, 95% B; 0.5–7 min, B linearly decreases from 95% to 65%; 7–8 min, B linearly decreases from 65% to 40%; 8–9 min, B is maintained at 40%; 9–9.1 min, B linearly increases from 40% to 95%; 9.1–12 min, B is maintained at 95%; the samples are kept at 4 °C in the autosampler throughout the analysis. To avoid interference caused by fluctuations in instrument detection signals, samples are analyzed in a random order. QC samples are inserted in the sample queue to monitor and evaluate the system's stability and the reliability of the experimental data. After sample detection, AB Triple TOF 6600 mass spectrometer is used to acquire the primary and secondary mass spectra of the samples. The ESI source conditions after HILIC chromatographic separation are as follows: Ion Source Gas1 (Gas1): 60, Ion Source Gas2 (Gas2): 60, Curtain gas (CUR): 30, source temperature: 600 °C, IonSpray Voltage Floating (ISVF): ± 5500 V (positive and negative modes); TOF MS scan m/z range: 60–1000 Da, product ion scan m/z range: 25–1000 Da, TOF MS scan accumulation time 0.20 s/spectra, product ion scan accumulation time 0.05 s/spectra; the secondary mass spectrometry is acquired by information-dependent acquisition (IDA) in high sensitivity mode, with Declustering potential (DP): ±60 V (positive and negative modes), Collision Energy: 35 ± 15 eV, and IDA settings as follows: Exclude isotopes within 4 Da, Candidate ions to monitor per cycle: 6. The raw MS data was first processed by converting it to MzXML files using ProteoWizard MSConvert and then analyzed using XCMS software for peak picking and grouping with specific parameters. CAMERA software was utilized for isotopes and adducts annotation. Only variables with >50% nonzero measurement values were retained in the extracted ion features. Compound identification was achieved by comparing accurate m/z values and MS/MS spectra with an in-house database containing authentic standards. The processed data underwent statistical analysis using the R package ropls, involving multivariate analysis such as PCA and OPLS-DA with 7-fold cross-validation and response permutation testing for model evaluation. Variable importance in the projection (VIP) values were calculated to assess their contribution to classification, and significance testing using Student's t test was conducted to identify significantly changed metabolites (VIP > 1 and p-value < 0.05). Pearson's correlation analysis was performed to evaluate variable relationships.

Flow cytometry analysis of *M. smegmatis* induced macrophage apoptosis

2×10^6 THP-1 cells were infected with WT_*Ms*, Δ*MSMEG_4702* and Δ*MSMEG_4702*::*Rv0102* for 6 h and 48 h. The infected cells were washed with ice-cold PBS and the apoptotic cells were determined by Annexin V-FITC and propidium iodide (PI) according to the manufacturer's instructions (Beibo, Shanghai, China). This product detects the externalization of phosphatidylserine in apoptotic cells using recombinant annexin V conjugated to green-fluorescent FITC dye and dead cells using propidium iodide (PI). The cells were subjected to fluorescence microscopy analysis and flow cytometry. Untreated cells were taken as negative control.

RT-PCR and assay for cytokines

PMA-differentiated THP-1 cells were infected with WT_*Ms*, Δ*MSMEG_4702* and Δ*MSMEG_4702*::*Rv0102* at an MOI of 10. After 6, 24 and 48 h infection, total cellular RNA was extracted from cells was extracted from the infected cells using RNA extraction kit (TIANGEN) according to the manufacturer's recommendations. cDNA synthesis was performed using the PrimeScript RT reagent kit (Takara, Shiga, Japan). Quantitative real-time RT-PCR reactions were performed using a CFX96 RT-PCR Detection System (Bio-Rad) using SYBR Green Master Mix. Relative mRNA levels were calculated after normalizing to β-actin. copperlture supernatants were collected from the infected macrophages, the cytokines production was detected with commercialy available ELISA kits for TNF-α, IL-10, IL-1β, IL-12, IL-6 and IL-8 (eBioscience).

Statistics and reproducibility

For data from growth curves, copper and zinc ion accumulation, and antibiotic sensitivity experiments, the mean and standard deviation of each experiment were calculated in order to compare changes between different

treatment groups. For multiple sets of data (such as bacterial growth and copper accumulation at different copper or zinc ion concentrations), one-way ANOVA or multivariate ANOVA were used to assess whether there were significant differences between treatment groups. Each experiment was repeated at least three times, and *T*-test statistical methods were used to analyze the data from the repeated experiments to ensure the reliability of the results. In data visualization, boxplot or line chart was used by GraphPad Prism, R and other software to show the distribution and trend of data in each group for preliminary comparison. Data were expressed as the mean ± SEM of at least three independent experiments. Statistical analysis was performed using GraphPad Prism 8.0. The results from RT-PCR, and CFU assays were analyzed by Student's *t* test. Differences were considered statistically significant with $^{*}P < 0.05$, $^{**}P < 0.01$, and $^{***}P < 0.001$.

Reporting summary

Further information on research design is available in the Nature Portfolio Reporting Summary linked to this article.

Data availability

The data supporting the results of this study are publicly available. Transcriptomic data of zebrafish have been deposited in the GEO database under the accession number GSE235754. Interested researchers can access and download the data from the GEO database. In addition, the metabolomics dataset was uploaded to the ENA-EBI database with the accession number MTBLS8036 and can be accessed and downloaded from the appropriate repository. Moreover, the full-size gel images have been included in Supplementary Fig. 12 and are also available for download. Source data underlying all figures can be found in Supplementary Data 1.

Abbreviations

Mtb	Mycobacterium tuberculosis
ROS	reactive oxygen species
NADH	Nicotinamide adenine dinucleotide
NCBI	national center for biotechnology information
PBS	phosphate buffer saline
LDH	lactate dehydrogenase
THP-1	human myeloid leukemia mononuclear cells
TSB	Tryptic soy broth
PMA	Phorbol-12-myristate-13-acetate
MOI	multiplicity of infection
SDS	Sodium dodecyl sulfate
LPS	Lipopolysaccharide
PAGE	polyacrylamide gelelectrophoresis
FBS	fetal bovine serum
CFU	Colony-Forming Units
LMP	lysosomal membrane permeability

Received: 12 March 2024; Accepted: 6 September 2024;
Published online: 19 September 2024

References

1. Mehdiratta, K. et al. Kupyaphores are zinc homeostatic metallophores required for colonization of mycobacterium tuberculosis. *Proc. Natl Acad. Sci. USA* **119**, e2110293119 (2022).
2. Kunkle, D. E. & Skaar, E. P. Moving metals: how microbes deliver metal cofactors to metalloproteins. *Mol. Microbiol.* **120**, 547–554 (2023).
3. Samanovic, M. I., Ding, C., Thiele, D. J. & Darwin, K. H. Copper in microbial pathogenesis: meddling with the metal. *Cell Host Microbe.* **11**, 106–115 (2012).
4. Bagcchi, S. WHO's global tuberculosis report 2022. *Lancet. Microbe.* **4**, e20 (2023).
5. Serafini, A. Interplay between central carbon metabolism and metal homeostasis in mycobacteria and other human pathogens. *Microbiology (Reading)* https://doi.org/10.1099/mic.0.001060 (2021).
6. Shey-Njila, O. et al. CtpB facilitates mycobacterium tuberculosis growth in copper-limited niches. *Int. J. Mol. Sci.* **23**, 5713 (2022).
7. Oikawa, S. & Kawanishi, S. Site-specific DNA damage induced by NADH in the presence of copper(II): role of active oxygen species. *Biochemistry* **35**, 4584–4590 (1996).
8. Tejeda, C. et al. Experimental evidence of the anti-bacterial activity pathway of copper ion treatment on mycobacterium avium subsp. paratuberculosis. *Braz. J. Microbiol.* **54**, 407–413 (2023).
9. Doku, R. T., Park, G., Wheeler, K. E. & Splan, K. E. Spectroscopic characterization of copper(I) binding to apo and metal-reconstituted zinc finger peptides. *J. Biol. Inorg. Chem.* **18**, 669–678 (2013).
10. Giachino, A. & Waldron, K. J. Copper tolerance in bacteria requires the activation of multiple accessory pathways. *Mol. Microbiol.* **114**, 377–390 (2020).
11. Neyrolles, O., Wolschendorf, F., Mitra, A. & Niederweis, M. Mycobacteria, metals, and the macrophage. *Immunol. Rev.* **264**, 249–263 (2015).
12. Ekici, S. et al. Intracytoplasmic copper homeostasis controls cytochrome c oxidase production. *mBio* **5**, e01055–01013 (2014).
13. Navarro, C. A., von Bernath, D., Martinez-Bussenius, C., Castillo, R. A. & Jerez, C. A. Cytoplasmic CopZ-like protein and periplasmic rusticyanin and AcoP proteins as possible copper resistance determinants in acidithiobacillus ferrooxidans ATCC 23270. *Appl Environ. Micro.* **82**, 1015–1022 (2016).
14. Leon-Torres, A., Novoa-Aponte, L. & Soto, C. Y. CtpA, a putative mycobacterium tuberculosis P-type ATPase, is stimulated by copper (I) in the mycobacterial plasma membrane. *Biometals* **28**, 713–724 (2015).
15. Marcus, S. A., Sidiropoulos, S. W., Steinberg, H. & Talaat, A. M. CsoR is essential for maintaining copper homeostasis in Mycobacterium tuberculosis. *PLoS ONE* **11**, e0151816 (2016).
16. Igbaria-Jaber, Y., Hofmann, L., Gevorkyan-Airapetov, L., Shenberger, Y. & Ruthstein, S. Revealing the DNA binding modes of CsoR by EPR spectroscopy. *ACS Omega* **8**, 39886–39895 (2023).
17. Turner, A. G., Ong, C. Y., Walker, M. J., Djoko, K. Y. & McEwan, A. G. Transition metal homeostasis in streptococcus pyogenes and streptococcus pneumoniae. *Adv. Micro. Physiol.* **70**, 123–191 (2017).
18. Fu, Y., Chang, F. M. J. & Giedroc, D. P. Copper transport and trafficking at the host bacterial pathogen interface. *Acc. Chem. Res* **47**, 3605–3613 (2014).
19. Lomize, M. A., Pogozheva, I. D., Joo, H., Mosberg, H. I. & Lomize, A. L. OPM database and PPM web server: resources for positioning of proteins in membranes. *Nucleic Acids Res.* **40**, D370–376, (2012).
20. Nandi, S. K. et al. Evidences for zinc (II) and copper (II) ion interactions with mycobacterium leprae HSP18: effect on its structure and chaperone function. *J. Inorg. Biochem.* **188**, 62–75 (2018).
21. Quistgaard, E. M., Low, C., Guettou, F. & Nordlund, P. Understanding transport by the major facilitator superfamily (MFS): structures pave the way. *Nat. Rev. Mol. Cell Bio.* **17**, 123–132 (2016).
22. Khalfaoui-Hassani, B. et al. Widespread distribution and functional specificity of the copper importer CcoA: distinct copper uptake routes for bacterial cytochrome c oxidases. *MBio* **9**, e00065–18 (2018).
23. Rowland, J. L. & Niederweis, M. Resistance mechanisms of mycobacterium tuberculosis against phagosomal copper overload. *Tuberculosis (Edinb.)* **92**, 202–210 (2012).
24. Roberts, C. A. et al. The suf iron-sulfur cluster biosynthetic system is essential in staphylococcus aureus, and decreased suf function results in global Metabolic defects and reduced survival in human neutrophils. *Infect. Immun.* **85**, e00100-17 (2017).
25. Garcia, P. S., Gribaldo, S., Py, B. & Barras, F. The SUF system: an ABC ATPase-dependent protein complex with a role in Fe-S cluster biogenesis. *Res. Microbiol.* **170**, 426–434 (2019).
26. Chen, Z. et al. Mycobacterial WhiB6 differentially regulates ESX-1 and the dos regulon to modulate granuloma formation and virulence in Zebrafish. *Cell Rep.* **16**, 2512–2524 (2016).
27. Tan, G. et al. Copper binding in IscA inhibits iron-sulphur cluster assembly in Escherichia coli. *Mol. Microbiol* **93**, 629–644 (2014).

28. Willemse, D. et al. Rv1460, a SufR homologue, is a repressor of the suf operon in Mycobacterium tuberculosis. *PLoS One* **13**, e0200145 (2018).
29. Wolschendorf, F. et al. Copper resistance is essential for virulence of Mycobacterium tuberculosis. *Proc. Natl Acad. Sci. USA* **108**, 1621–1626 (2011).
30. Galle, J. N., Fechtner, T., Eierhoff, T., Romer, W. & Hegemann, J. H. A Chlamydia pneumoniae adhesin induces phosphatidylserine exposure on host cells. *Nat. Commun.* **10**, 4644 (2019).
31. Chow, S. H., Deo, P. & Naderer, T. Macrophage cell death in microbial infections. *Cell Microbiol.* **18**, 466–474 (2016).
32. Pan, H. et al. gene mediates innate immunity to tuberculosis. *Nature* **434**, 767–772 (2005).
33. Divangahi, M. et al. Mycobacterium tuberculosis evades macrophage defenses by inhibiting plasma membrane repair. *Nat. Immunol.* **10**, 899–U123 (2009).
34. Pagan, A. J. et al. mTOR-regulated mitochondrial metabolism limits mycobacterium-induced cytotoxicity. *Cell* **185**, 3720–3738.e3713 (2022).
35. Collins, S. L. et al. mTORC1 signaling regulates proinflammatory macrophage function and metabolism. *J. Immunol.* **207**, 913–922 (2021).
36. Dong, H. et al. ESAT6 inhibits autophagy flux and promotes BCG proliferation through MTOR. *Biochem. Biophys. Res. Commun.* **477**, 195–201 (2016).
37. Hasan, M. et al. Chronic innate immune activation of TBK1 suppresses mTORC1 activity and dysregulates cellular metabolism. *Proc. Natl Acad. Sci. USA* **114**, 746–751 (2017).
38. Parker, D. et al. Streptococcus pneumoniae DNA initiates type I interferon signaling in the respiratory tract. *mBio* **2**, e00016–00011 (2011).
39. Sekheri, M., Rizo-Tellez, S. A., Othman, A., El Kebir, D. & Filep, J. G. Interferon-beta regulates proresolving lipids to promote the resolution of acute airway inflammation. *Proc. Natl Acad. Sci. USA* **119**, e2201146119 (2022).
40. Xu, J. et al. A unique mycobacterium ESX-1 protein co-secretes with CFP-10/ESAT-6 and is necessary for inhibiting phagosome maturation. *Mol. Microbiol.* **66**, 787–800 (2007).
41. Wagner, D. et al. Elemental analysis of mycobacterium avium-, mycobacterium tuberculosis-, and mycobacterium smegmatis-containing phagosomes indicates pathogen-induced microenvironments within the host cell's endosomal system. *J. Immunol.* **174**, 1491–1500 (2005).
42. Speer, A., Rowland, J. L., Haeili, M., Niederweis, M. & Wolschendorf, F. Porins increase copper susceptibility of mycobacterium tuberculosis. *J. Bacteriol.* **195**, 5133–5140 (2013).
43. Lawton, T. J., Kenney, G. E., Hurley, J. D. & Rosenzweig, A. C. The CopC family: structural and bioinformatic insights into a diverse group of periplasmic copper binding proteins. *Biochemistry* **55**, 2278–2290 (2016).
44. Gupta, D. D. et al. Identification of a copper ion recognition peptide sequence in the subunit II of cytochrome c oxidase: a combined theoretical and experimental study. *J. Biol. Inorg. Chem.* **26**, 411–425 (2021).
45. Tsvetkov, P. et al. Copper induces cell death by targeting lipoylated TCA cycle proteins. *Science* **375**, 1254–1261 (2022).
46. Rojas-Espinosa, O. et al. A neutrophil-based test as an auxiliary tool for substantiating the diagnosis of bovine tuberculosis. *Int. J. Mycobacteriol.* **11**, 190–198 (2022).
47. Dubey, R. K. Assuming the role of mitochondria in mycobacterial infection. *Int. J. Mycobacteriol.* **5**, 379–383 (2016).
48. Murry, J. P., Sassetti, C. M., Lane, J. M., Xie, Z. & Rubin, E. J. Transposon site hybridization in Mycobacterium tuberculosis. *Methods Mol. Biol.* **416**, 45–59 (2008).
49. Liu, Y. G. & Chen, Y. High-efficiency thermal asymmetric interlaced PCR for amplification of unknown flanking sequences. *Biotechniques* **43**, 649–650 (2007).

Acknowledgements

This work was supported by Chongqing Postdoctoral Science Foundation (7820100597), Natural Science Foundation [grant numbers 82072246, 82211530059], 2023 key Disciplines On Public Health Construction in Chongqing No. CSTB2024NSCQ-MSX0703 No. 2023MSXM107.

Author contributions

J.X., S.M., Y.H., Q.Z., L.H., H.X., Ismail., P.L., Z.J. and J.X. analyzed the data. J.X., Z.W. and J.X. designed the study and wrote the paper. All authors have read and approved the manuscript.

Competing interests

The authors declare no competing interests.

Ethics

Animal Ethics Committee of Southwest University. All procedures were conducted in accordance with relevant guidelines and regulations. The animals used in this study were zebrafish (Danio rerio), with an age range of ~2–12 months and an average weight of 10 g. A total of 200 individuals of each sex (male and female) were included in the experiments.

Additional information

Supplementary information The online version contains supplementary material available at https://doi.org/10.1038/s42003-024-06860-9.

Correspondence and requests for materials should be addressed to Peibo Li, Zhijian Wang or Jianping Xie.

Peer review information *Communications Biology* thanks Krishna Kurthkoti and the other, anonymous, reviewer for their contribution to the peer review of this work. Primary Handling Editors: Karthika Rajeeve and Tobias Goris. A peer review file is available.